Engineering Geology 364 (2026) 108616

Contents lists available at ScienceDirect

Engineering Geology

journal homepage: www.elsevier.com/locate/enggeo

Hybrid SDF-CFD-DEM analysis of suffusion behavior in coral sand incorporating irregular particle morphology and intraparticle voids

Shuai Huang [b,c], Pei Wang [a,d,*], Zhengshou Lai [c,e,f], Zhen-Yu Yin [b], Linchong Huang [c,e,f], Changjie Xu [a,d]

[a] State Key Laboratory of Safety and Resilience of Civil Engineering in Mountain Area, East China Jiaotong University, Nanchang, 330013, Jiangxi, China
[b] Department of Civil and Environmental Engineering, The Hong Kong Polytechnic University, Hung Hom, Kowloon, Hong Kong, China
[c] State Key Laboratory of Tunnel Engineering, Guangzhou, 510275, China
[d] Institute of Geotechnical Engineering, School of Civil Engineering and Architecture, East China Jiaotong University, Nanchang, Jiangxi, China
[e] School of Civil Engineering, Sun Yat-sen University, Guangzhou 510275, China
[f] Guangdong Key Laboratory of Marine Civil Engineering, School of Civil Engineering, Sun Yat-sen University, Guangzhou 510275, China

ARTICLE INFO

Keywords:
Coral sand
Suffusion
CFD-DEM
Intraparticle voids
Particle morphology
Signed distance field

ABSTRACT

Coral sand is one of the common marine geomaterials characterized by highly irregular particle morphology and abundant intraparticle voids. The influences of the complex shape and intraparticle voids on the suffusion behavior of coral sand remains insufficiently understood. This work develops a numerical modeling framework that integrates a hybrid resolved and semi-resolved signed distance field (SDF) enhanced computational fluid dynamics (CFD) and discrete element method (DEM) approach for simulating suffusion in coral sand, accounting for both the irregular particle morphology and intraparticle voids. The framework employs the level set (LS) to represent intraparticle voids and spherical harmonics (SH) to capture apparent particle shapes, with a fully resolved scheme for coarse particles and a semi-resolved scheme for fine particles to balance accuracy and computational efficiency. The hybrid CFD-DEM scheme for coral sand is validated through the simulations of particle settling and Ergun's tests. Comprehensive numerical simulations are performed to evaluate the effects of intraparticle voids and particle shape on the suffusion behavior. The results reveal that intraparticle voids inhibit suffusion by trapping fine particles. In contrast, the simplified spherical particle representations, which is commonly adopted in previous studies, will significantly overestimate fine particle erosion during suffusion processes. Furthermore, a sensitivity analysis is conducted to assess the influence of flow velocity and direction, indicating that increased inlet velocity enhances fines erosion, whereas flow directions deviating from gravity reduce erosion efficiency. These findings highlight the importance of particle morphology and intraparticle voids for accurate prediction of suffusion behavior in coral sand, and the proposed framework provides a reliable analysis tool with high physical fidelity for investigating suffusion mechanisms in complex granular systems.

1. Introduction

Coral sand is a common type of geomaterial formed from the remains of marine organisms, which is widely distributed on tropical islands and reefs (e.g., the SouthChina Sea, the Persian Gulf, and the Red Sea) (Alba and Audibert, 1999). The abundance of coral sands in shallow marine environments has driven their extensive use as cost-effective fill materials in offshore engineering projects, such as artificial island construction, airport runways, and submarine pipeline foundations (Wang et al., 2011, 2017; Chao et al., 2024, 2025). Comparing with terrigenous quartz sand, coral sand is characterized by two distinct features: highly irregular particle morphology and well-developed intraparticle voids (Wang et al., 2020). These characteristics have been recognized as the primary cause of the high crushability and unique compression behavior of carbonate sediments (Coop, 1990; Golightly and Hyde, 2021). The mechanical and hydromechanical properties of coral sand is influenced by its special morphological characteristics. For example, Wang et al. (2019) suggested that the shear behavior of coral sand are related to the confining pressure. Under lower confining pressures, the irregular apparent shape of the particles produces

* Corresponding author at: State Key Laboratory of Safety and Resilience of Civil Engineering in Mountain Area, East China Jiaotong University, Nanchang, 330013, Jiangxi, China.
E-mail address: peiwang@ecjtu.edu.cn (P. Wang).

https://doi.org/10.1016/j.enggeo.2026.108616
Received 6 July 2025; Received in revised form 7 February 2026; Accepted 8 February 2026
Available online 9 February 2026

particle obstruction, which leads to shear dilation and increases the shear strength. However, significant particle breakage is observed at higher confining pressures, which decreases the shear strength. The intraparticle voids of coral sand significantly reduce the strength and effective modulus with a logarithmic decreasing trend (Lv et al., 2021). In terms of hydromechanical properties, the permeability of coral sands is positively correlated with the grain size, which is concluded by Fan et al. (2021) through X-ray computed tomography (CT) scanning and pore network modeling. In addition, the internal erosion behavior in coral sand is also affected by the intraparticle voids, which makes the flow path more complex (Wang et al., 2022b). Field investigations have reported foundation settlement and even collapse in hydraulic-filled coral-reef islands due to seepage-induced internal erosion (Ding et al., 2024). It requires a fundamental understanding of the behavior of coral sands to facilitate the construction of foundation engineering in coral reefs.

Suffusion is a major type of internal erosion, which refers to the process of fine particles being transported away from the pores of the coarse particle skeleton under the action of seepage. This phenomenon usually occurs in the gap-graded soils, and can lead to structural damage, permeability variations, and even geologic hazards (Sibille et al., 2015; Mehdizadeh et al., 2017; Xiong et al., 2021b). The internal stability of gap-graded soils was first systematically evaluated through geometric criteria (Kenney and Lau, 1985) and hydraulic-based assessments (Skempton and Brogan, 1994). These pioneering works established the fundamental understanding of how the soil skeleton constrains fine particle migration. The susceptibility to suffusion in coral sand presents intrinsic differences when compared to terrigenous siliceous sands. While the erodibility of siliceous sand is primarily governed by its initial particle size distribution and matrix stability (as its high stiffness minimizes particle breakage under common engineering stresses), coral sand exhibits an inherently high crushability due to its porous, hollow, and weak skeletal structure (Li et al., 2024, 2025). This unique crushable nature significantly influences the erodibility of material and the development of suffusion. In the marine environment where coral reefs are located, frequent and complex loading effects such as waves, storm surges, and seismic excitation can induce substantial particle breakage in coral sands (Wang et al., 2019, 2021, 2022a, 2025a). This breakage is a dynamic process that generates a large number of fine particles in situ, continuously modifying the particle size distribution and contributing to the development of gap-graded structures (Xin et al., 2024). This mechanism of dynamic supply of fines is the key distinction from siliceous sands, leading to a more complex and progressive suffusion process in coral sand. The subsequent redistribution of these newly generated fines causes changes in the microstructure. This process alters local contact networks and pore connectivity. Consequently, both the mechanical behavior and seepage pathways are affected. Furthermore, seawater flow will increase the pore water pressure and form hydraulic gradient, which further aggravates the suffusion of fine particles, thus posing a significant risk to the stability of coral sand foundations (Xiong et al., 2023a,b). The unique morphological features of coral sands (e.g., highly complex particle morphology and intraparticle voids) further complicate fluid flow behavior. The rough surfaces may lead to localized flow disruptions, while the intraparticle voids create additional fluid channels. This further affect the migration and clogging behavior of fines during suffusion. Therefore, it is necessary to carry out a deep study incorporating the realistic morphological characteristics of coral sand to more accurately assess their suffusion response.

To investigate the suffusion mechanisms of granular materials, scholars have progressed from fundamental experimental observations to high-fidelity numerical frameworks. Early experimental programs, notably the pioneering tests by Skempton and Brogan (1994) and Fannin and Moffat (2006), established the foundational understanding of the hydromechanical triggers and stress-reduction effects during suffusion. Subsequent laboratory investigations (Ke and Takahashi, 2014a; Nguyen et al., 2019; Kodieh et al., 2021) have further expanded these insights by examining the diverse hydromechanical responses and microstructural evolutions of suffusion. Complementing these experimental insights, numerical frameworks have emerged as a robust alternative for investigating suffusion mechanisms (Galindo-Torres et al., 2015; Xiong et al., 2021b,a; Chen et al., 2023; Wang et al., 2024, 2025b). Numerical simulations can provide more advanced insights into the suffusion behavior at the microscopic level, such as particle migration, fluid flow field, and particle–fluid interactions. The coupled computational fluid dynamics (CFD) and discrete element method (DEM) is a powerful numerical tool for suffusion problem (Cundall and Strack, 1979; Goniva et al., 2010; Hager et al., 2014), and has been employed in coral sands in recent years. For instance, Xiong et al. (2023a,b) examined the suffusion behavior of calcareous sand under reversed hydraulic cycling, tidal fluctuations, and traffic loads based on the CFD-DEM method. It should be noted that these studies used the spherical particle model to simplify the characterization of coral sands. It is widely recognized that the mechanical behavior of granular materials can be significantly affected by the particle shape (Lai et al., 2020; Wang et al., 2023). This simplification neglects the irregular apparent shape and intraparticle voids of coral sand, the implications of which for the prediction of fines erosion are not clearly understood. Furthermore, Wang et al. (2022b) adopted the dynamic fluid mesh (DFM) approach to account for intraparticle fluid flow by embedding virtual voids within coarse particles, allowing fluid to pass through. Nevertheless, the coral sand particles are still represented in the solid phase by spherical particles. Therefore, there is a gap in the existing suffusion simulations of coral sand that directly consider the irregular particle shape and intraparticle voids.

Recently, there have been several studies that extend CFD-DEM approach to simulate the suffusion of irregular-shaped particles, which have provided valuable insights into fluid–particle interactions under more realistic morphological conditions (Xiong et al., 2021a; Liu et al., 2024; Liu and Yin, 2024). For instance, Xiong et al. (2021a) investigated the effect of particle shape on suffusion behavior using an unresolved CFD-DEM approach. In addition, Liu et al. (2024) employed the resolved CFD-DEM approach to simulate suffusion in gap-graded granular soils with non-spherical particles. It should be pointed out that the particle geometries in these studies are limited to convex shapes. Moreover, the unresolved CFD-DEM approach remains immature in accurately estimating drag forces on irregular particles. To further address these issues, Liu and Yin (2024) conducted a suffusion simulation of particles with concave shapes using the resolved CFD-DEM approach. The concave particles were implemented with the sphere clump model. However, the clumps particle model is computationally expensive when modeling the complex particle morphology, and is difficult to characterize porous media. To improve the physical fidelity of suffusion simulations in coral sand, the morphology of real coral sand particles should be accurately represented.

At present, X-ray CT is the most prevalent method for directly obtaining three-dimensional morphological information, and has been successfully applied to the characterization of coral sand Kong and Fonseca (2019). Utilizing coral sand particles reconstructed from X-ray CT data, Huang et al. (2023) presented a DEM modeling of coral sand in consideration of both the irregular shape and intraparticle voids of particles. This work effectively addresses the challenge of coral sand modeling with realistic shapes in the DEM framework. In addition, Lai et al. (2023) proposed a signed distance field (SDF) enhanced fully resolved CFD-DEM for simulation of granular flows involving multiphase fluids and irregularly shaped particles. These previous efforts (Huang et al., 2023; Lai et al., 2023) collectively provide a solid foundation for extending CFD-DEM modeling to coral sands by incorporating both irregular shape and intraparticle voids. The resolved CFD-DEM approach enables fine-scale modeling of fluid–particle interactions, which is particularly beneficial for accurately evaluating the hydrodynamics of coral sand particles with complex geometries.

However, due to the small size of fine particles involved in suffusion, fully resolved simulations typically require extremely fine fluid meshes, resulting in prohibitive computational costs. In contrast, unresolved approach are generally more computationally efficient, but the lack of accurate drag force models tailored for irregular coral sand particles compromises the reliability of particle–fluid interactions calculations. To bridge the gap between resolved and unresolved approaches, a semi-resolved CFD-DEM approach has been developed recently (Wang and Liu, 2021; Chen and Zhang, 2022). The semi-resolved scheme offers a moderate approach by applying corrections based on neighboring fluid information. Such flexibility permits a wider ratio between the fluid mesh and particle size, making it particularly suitable for systems containing a range of intermediate particle sizes. Accordingly, the option of CFD-DEM coupling approach is crucial to balance the accuracy and computational feasibility of suffusion simulations in coral sand.

This study addresses the critical challenge of accurately simulating suffusion in biogenic coral sand, where traditional spherical particle models fail to capture the influence of irregular morphology and well-developed intraparticle voids. To overcome this limitation, a novel numerical modeling framework for coral sand suffusion is developed. This framework introduces a hybrid resolved and semi-resolved SDF-CFD-DEM approach. The coral sand particles are represented using two particle models, namely level set (LS) and spherical harmonics (SH). The effects of intraparticle voids, particle shape, and variations in flow velocity and flow direction on the suffusion process are systematically investigated. The rest of the paper is organized as follows. Section 2 introduces the hybrid resolved and semi-resolved SDF-CFD-DEM modeling framework for coral sand. Section 3 presents the validation of the hybrid model for suffusion simulations in coral sand using particle settling and Ergun's tests. Section 4 describes the setup of the numerical suffusion model. Section 5 analyzes the simulation results. Section 7 summarizes the concluding remarks.

2. Hybrid resolved and semi-resolved SDF-CFD-DEM modeling for coral sand

2.1. Characterization of coral sand morphology

Coral sand exhibits intricate morphological features, characterized by highly complex shapes and fully developed intraparticle voids. The rising popularity of X-ray CT in coral sand morphology characterization stems from its ability to directly capture comprehensive three-dimensional morphological information (Andò et al., 2013; Kong and Fonseca, 2019; Huang et al., 2023). In our previous work (Huang et al., 2023), we utilized the X-ray CT and image processing to effectively reconstruct the particle shapes of coral sand. The processing flow is briefly described herein for the sake of completeness, whereas interested readers are referred to Huang et al. (2023) for more details. As illustrated in Fig. 1, a number of lump-like coral sand particles are separated by silicone gel and packed into a cylindrical container prepared for X-ray CT scan. Then, the raw CT images are undergo two image processing schemes to respectively reconstruct the apparent shapes and intraparticle voids of coral sand particles. The example particles with and without intraparticle voids are shown in Fig. 1. It is important to highlight that the two variations of coral sand particles are intended to be specifically employed to investigate the effect of intraparticle voids on the suffusion mechanism.

2.2. SDF-DEM model for coral sand

The SDF-DEM method, recently proposed by Lai et al. (2022), is applicable to arbitrary-shaped particles and has achieved DEM modeling of coral sand with intraparticle voids (Huang et al., 2023). In DEM, particle motion is governed by the Newton-Euler equation as

$$m\frac{\partial \boldsymbol{u}_p}{\partial t} = m\boldsymbol{g} + \boldsymbol{F}_c + \boldsymbol{F}_f \tag{1}$$

$$\boldsymbol{I}\frac{\partial \boldsymbol{\omega}_p}{\partial t} + \boldsymbol{\omega}_p \times (\boldsymbol{I}\boldsymbol{\omega}_p) = \boldsymbol{M}_c + \boldsymbol{M}_f \tag{2}$$

where $\boldsymbol{u}_p$ and $\boldsymbol{\omega}_p$ are particle translation and rotation velocities, m and $\boldsymbol{I}$ are particle mass and moment of inertia tensor, and $\boldsymbol{F}_c$, $\boldsymbol{M}_c$, $\boldsymbol{F}_f$, and $\boldsymbol{M}_f$ are the contact force, contact moment, fluid force, and force moment experienced by the particle, respectively.

In the SDF-DEM, particles are described by SDF-based generic interface with two functions: the SDF function and surface projection function. The SDF function maps a spatial point to a signed value, assumed positive inside a particle and negative outside (Lai et al., 2022). The zeroth isosurface of SDF thus represents the particle surface. The surface projection function projects a point onto the particle surface to determine the contact point. With particles described by SDF, the node-to-surface contact algorithm detects contacts and resolves contact geometric features. The energy-conserving contact theory originally proposed by Feng (2021) is adopted for the evaluation of contact behavior.

In the work of Huang et al. (2023), the coral sand particles with and without intraparticle voids are effectively represented by the SDF-based LS and SH particle models, respectively. More specifically, the LS particle model utilizes a grid of discretized SDF values and their interpolation to define the SDF field, which can be directly created by the CT data of coral sand particles, aiding to capture of intraparticle voids in high-fidelity. The SH particle model has been widely applied to model irregular shaped particles in three-dimensions, which can accurately represent the apparent shape of coral sand. Fig. 2 illustrates the generation process of SDF-based LS and SH particle models for the example particle in Fig. 1. It should be noted that both the LS and SH particle models have a parameter (i.e., grid resolution for LS and degree for SH) that can be flexibly adjusted to weigh a balance between shape representation accuracy and computational efficiency. According to Huang et al. (2023), the LS resolution of 200 μm and SH degree of 10 are adopted in this work. The visualization of the LS and SH particles in Fig. 2 demonstrates the accurate reconstruction of both the primary intraparticle voids and the apparent shape.

2.3. Hybrid resolved and semi-resolved CFD-DEM schemes for suffusion

2.3.1. Formulation of CFD

Considering two-phase incompressible fluids in this work, the continuity and momentum equations are given as

$$\frac{\partial(\epsilon\rho_f)}{\partial t} + \nabla\cdot\left(\epsilon\rho_f\boldsymbol{u}_f\right) = 0 \tag{3}$$

$$\frac{\partial(\epsilon\rho_f\boldsymbol{u}_f)}{\partial t} + \nabla\cdot(\epsilon\rho_f\boldsymbol{u}_f\otimes\boldsymbol{u}_f) = -\epsilon\nabla p + \epsilon\nabla\cdot(\mu_f\nabla\otimes\boldsymbol{u}_f) + \epsilon\rho_f\boldsymbol{g} + \boldsymbol{f}_t + \boldsymbol{f}_p \tag{4}$$

where $\boldsymbol{u}_f$ represents fluid velocity, p is pressure, ρ_f denotes fluid density, ϵ accounts for porosity due to particles or a porous solid matrix, μ_f is dynamic viscosity, $\boldsymbol{g}$ is gravitational coefficient, $\boldsymbol{f}_t$ represents surface tension force at phase interfaces, and $\boldsymbol{f}_p$ represents interaction force from solid particles, evaluated by different schemes based on the particle–fluid size ratio. The volume of fraction method is employed to average properties of different phases, and the interface is tracked using level set methods.

2.3.2. Resolved CFD-DEM

The resolved CFD-DEM shall be used to solve fluid–particle interactions directly and fully, employing a fine fluid mesh to consider the shape of particles. Recently, Lai et al. (2023) proposed a novel SDF-CFD-DEM approach for numerical modeling of fluid–particle systems, showcasing the capability to simulate the interaction of multiphase fluids and irregularshaped particles. In SDF-CFD-DEM, the fluid–particle interaction is resolved by the immersed boundary method (IBM), which assumes a fictitious CFD domain in the space occupied by the DEM particles. Specifically, the impact of particles on fluids are accounted for

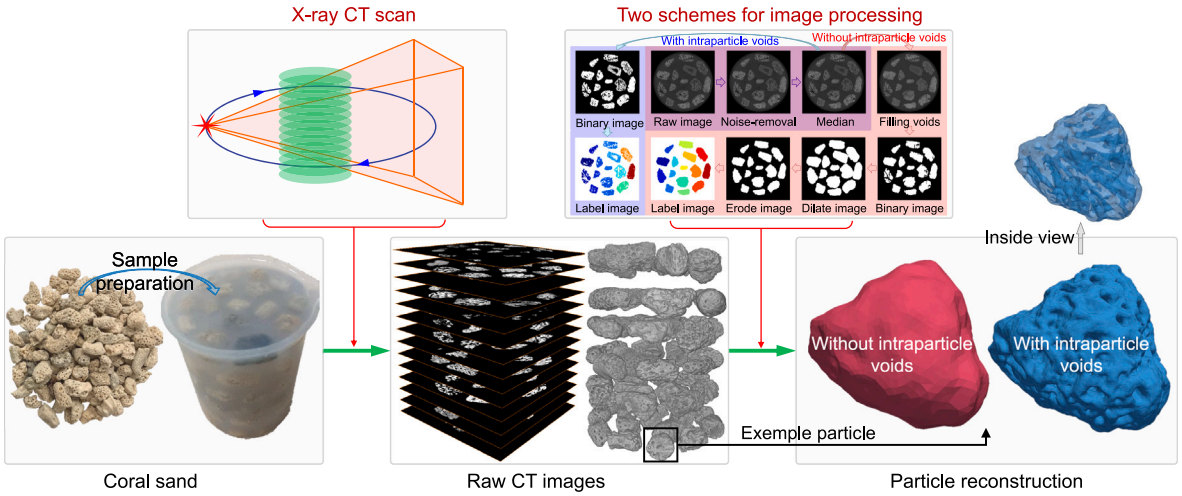

Fig. 1. Schematic illustration of coral sand reconstruction using X-ray scan and image processing.
Source: Modified from Huang et al. (2023).

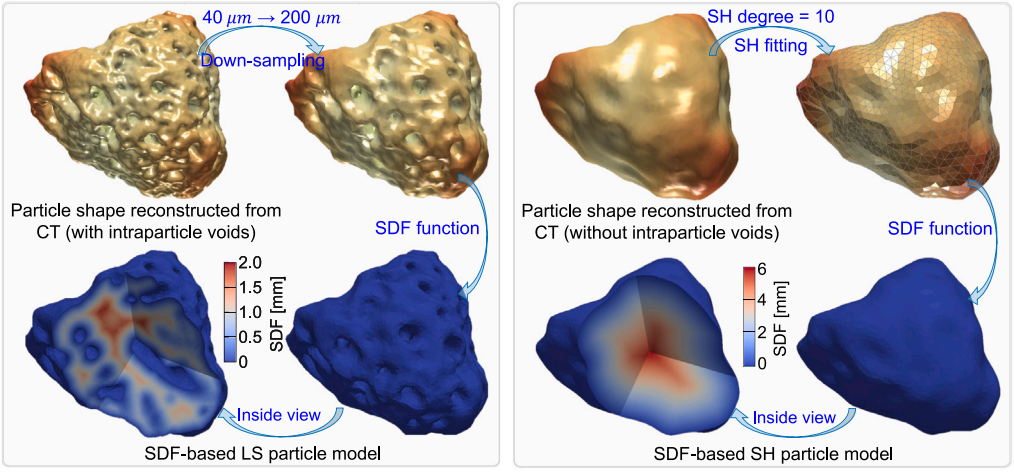

(a) (b)

Fig. 2. Illustration of (a) SDF-based LS particle model, and (b) SDF-based SH particle model for coral sand.

by adding the IBM-related source terms to the fluid governing equations and calculating fluid forces on particles by integrating stresses over particle surfaces. The IBM-related source force $\boldsymbol{f}_{IB}$ is calculated as

$$\boldsymbol{f}_{IB} = (\hat{\boldsymbol{u}}_f - \boldsymbol{u}_f)/A_u \tag{5}$$

where A_u is a coefficient derived from the momentum equation (4). Specifically, in the context of the *OpenFOAM* library, the left-hand side of Eq. (4) can be split into $A_u\boldsymbol{u} - H$, where $A_u\boldsymbol{u}$ and H represent the implicit and explicit parts of the momentum, respectively (Nan et al., 2022). The source force $\boldsymbol{f}_{IB}$ is employed to correct the velocity of fluid cells overlapped by particles to align with the particle velocities, which can be expressed as

$$\hat{\boldsymbol{u}}_f = (1-\varphi_s)\boldsymbol{u}_f + \varphi_s\boldsymbol{u}_s \tag{6}$$

where $\varphi_s = \phi_s\rho_s/\rho$ represents the density-weighted solid fraction, with ρ being the averaged density, and $\boldsymbol{u}_s$ represents the solid velocity interpolated at the cell center, calculated as

$$\boldsymbol{u}_s = \boldsymbol{u}_p + \boldsymbol{\omega}_p \times (\boldsymbol{x}_i - \boldsymbol{x}_p) \tag{7}$$

$$\rho = (1-\phi_s)\rho_f + \phi_s\rho_s \tag{8}$$

where $\boldsymbol{x}_i$ is the mesh cell center, $\boldsymbol{x}_p$ is the particle centroid, and $\boldsymbol{u}_p$ and $\boldsymbol{\omega}_p$ are the particle velocity and spin, respectively. Additionally, ρ_s represents the particle density, and ϕ_s denotes the cell solid fraction.

The force applied onto particles by the fluids is integrated from the fluid forces that act on the surfaces of a particle (Yang and Balaras, 2006). This integration, after applying the divergence theorem, is calculated as

$$\boldsymbol{F}_f = \sum^{cells} \left(\varphi_s \nabla\cdot\boldsymbol{\sigma} - (1-\varphi_s)\boldsymbol{f}_{IB}\right) V_c \tag{9}$$

$$\boldsymbol{M}_f = \sum^{cells} (\boldsymbol{x}_i - \boldsymbol{x}_p) \times \left(\varphi_s \nabla\cdot\boldsymbol{\sigma} - (1-\varphi_s)\boldsymbol{f}_{IB}\right) V_c \tag{10}$$

where $\sum^{cells}$ indicates the summation over all mesh cells that are overlapped by a particle, and V_c is the cell volume. The term $(1-\varphi_s)\boldsymbol{f}_{IB}$ accounts for errors due to the averaging effects of fluid and solid velocities at partially overlapped cells.

In this work, we use the fully resolved SDF-CFD-DEM approach to model the interaction of fluids and the coral sand particles with intraparticle voids. The critical aspect of this numerical simulation is to accurately characterize the particle shape of coral sand, including intraparticle voids, within CFD. This entails the precise determination of the solid fraction of the fluid cells overlapped by particles. The SDF-based estimation approach in the SDF-CFD-DEM is utilized to evaluate of solid fraction. Specifically, the solid fraction is determined by calculating the fraction of the summation of the SDF values of the cell nodes inside particles to the summation of the absolute SDF values of all cell

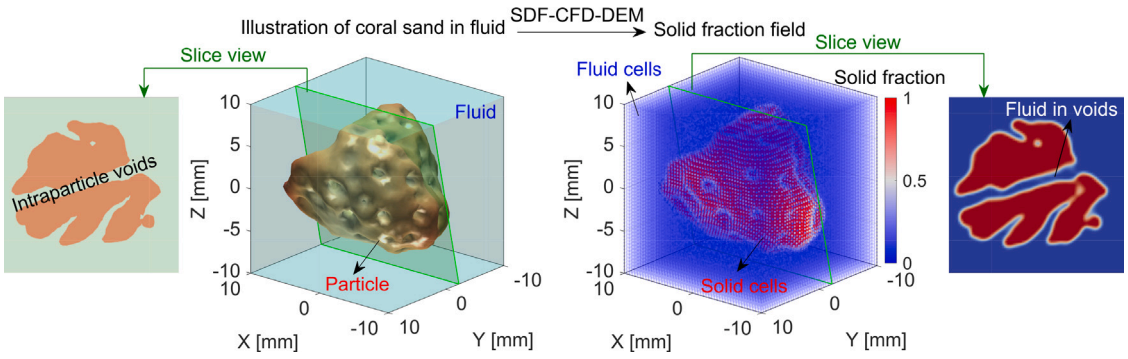

Fig. 3. Illustration of solid fraction field for coral particle with intraparticle voids. (For interpretation of the references to color in this figure legend, the reader is referred to the web version of this article.)

nodes. Coral sands are described by the SDF-based particle models, as shown in Fig. 2, enabling the efficient and accurate estimation of the solid fraction. Fig. 3 visualizes the solid fraction field for coral particle with intraparticle voids. In an illustrative setup, a example coral sand particle is positioned within a cubic fluid domain, as depicted in the left schematic of Fig. 3. Subsequently, it is modeled utilized the SDF-CFD-DEM approach, showcasing the solid fraction field on the right side of Fig. 3. The blue area signifies the fluid cells, while the red area denotes the solid cells, demonstrating the accurate representation of coral sand morphology within the CFD fluid. Moreover, one can observe the precise depiction of the intraparticle voids of coral sand by comparing slices of the particle and solid fraction fields. Notably, the particle–fluid mesh size ratio is 30 for simulating fluid entry the intraparticle voids.

2.3.3. Semi-resolved CFD-DEM

The semi-resolved CFD-DEM scheme is developed based on the unresolved CFD-DEM for dealing with moderately fine particles (Wang and Liu, 2021; Chen and Zhang, 2022). It mainly addresses the difficulty of the unresolved scheme in accurately calculating the drag force when the particle–fluid mesh size ratio ranges from 1/3 to 8. In the unresolved CFD-DEM scheme, the fluid–particle intersection forces consist of drag and buoyant force. The source force induced by them is calculated as:

$$\boldsymbol{f}_p = \frac{1}{V_c}\sum^{p}\left(\boldsymbol{F}_{drag} + \boldsymbol{F}_{buoy}\right) \tag{11}$$

where $\sum^{p}$ indicates the summation of all particles within a fluid cell. Buoyant force $\boldsymbol{F}_{buoy} = -V_p\nabla p$, with V_p is the particle volume, ∇p and is the pressure gradient. Drag force $\boldsymbol{F}_{drag}$ is calculated as:

$$\boldsymbol{F}_{drag} = \hat{f}_{drag}\left(3\pi\epsilon\mu_f d\boldsymbol{u}_{rel}\right) \tag{12}$$

where $\boldsymbol{u}_{rel} = \boldsymbol{u}_p - \boldsymbol{u}_f/\epsilon$ is the relative velocity of the particle to the fluid and d is the particle size. $\hat{f}_{drag}$ is the drag factor, evaluated by the Gidaspow's model (Sobieski, 2009), which combines Ergun's model (Ergun and Orning, 1949) for dense systems and Wen-Yu's model (Wen and Yu, 1966) for dilute systems.

$$\hat{f}_{drag} = \begin{cases} \frac{150(1-\epsilon)}{18\epsilon^2} + \frac{1.75}{18\epsilon^2}Re & \epsilon \le 0.8 \\ \frac{C_d}{24}Re\epsilon^{-3.65} & \epsilon > 0.8 \end{cases} \tag{13}$$

$$C_d = \begin{cases} \frac{24}{Re}\left(1 + 0.15Re^{0.687}\right) & Re \le 1000 \\ 0.44 & Re > 1000 \end{cases} \tag{14}$$

where Re is the Reynolds' number, ϵ is the fluid volume fraction, C_d represents the drag coefficient. It should be pointed out that the Gidaspow's model is derived based on the assumption of spherical particles. In this work, the irregular shape fine particles are also considered

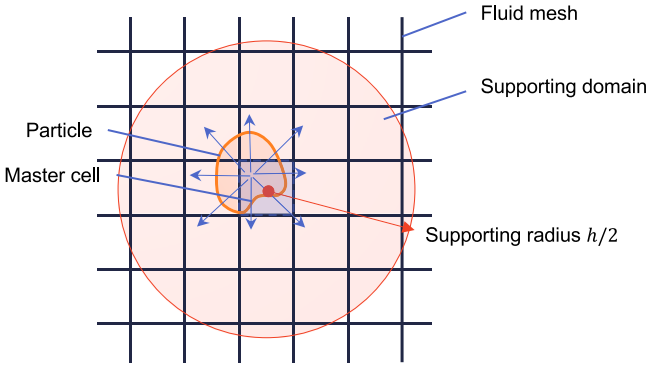

Fig. 4. Illustration of the kernel approximation in semi-resolved CFD-DEM scheme.

in the CFD-DEM model. However, the irregular shape of fine particles is retained primarily to ensure the accuracy of inter-particle contact mechanics and initial packing structure within the DEM scheme, as this shape realism is critical for suffusion. The fluid–particle drag component is simplified using Gidaspow's model based on the volume-equivalent diameter. The development of drag models for irregularly shaped particles remains a major challenge in the field. There have been some beneficial explorations in this area (He et al., 2016; Wang et al., 2018; Hwang et al., 2024). For instance, He et al. (2016) adopted a modified Gidaspow's model that incorporated particle sphericity to achieve improved accuracy. Machine learning approaches also offer a promising avenue for exploring and parameterizing the drag coefficient for complex geometries (Hwang et al., 2024).

It should be noted that the unresolved scheme has a limitation on the fluid–particle size ratio (e.g. < 1/3), and the accuracy of the simulation may be lost beyond the limitation. For particles with sizes comparable to or even larger than the size of fluid cells, the semi-resolved scheme is an optimal choice. Specifically, the semi-resolved scheme employs the kernel-based approximation approach to extend the influential domain of particle from the particle master CFD cell to the supporting domain with diameter h, as shown in Fig. 4. This extension allows for the interpolation of void fraction and fluid velocity from fluid cells within the supporting domain. Additionally, by interpolating fluid properties for drag force calculation and distributing the drag force to neighboring cells, the fluid–particle interaction becomes more accurate for moderately fine particles, enabling the use of the unresolved CFD–DEM approach.

In this work, the kernel function is adopted as

$$\delta = \begin{cases} \frac{1}{8}\left(3 - 2r + \sqrt{1 + 4r - 4r^4}\right) & r \le 1 \\ \frac{1}{8}\left(5 - 2r - \sqrt{-7 + 12r - 4r^4}\right) & 1 < r \le 2 \end{cases} \tag{15}$$

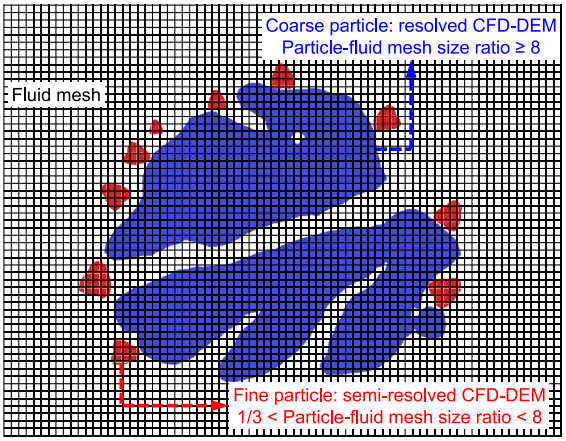

Fig. 5. Hybrid schemes of resolving fluid–particle interaction.

where δ is the calculated weight and $r = 2d/h$ is the normalized radial distance, with d being the distance from a given position to the center of the supporting domain and h being the size (i.e., diameter) of the supporting domain.

2.3.4. Hybrid schemes

In this work, the hybrid resolved and semi-resolved SDF-CFD-DEM is utilized for the simulation of suffusion process of coral sand. As illustrated in Fig. 5, there are both coarse and fine particles in the fluid domain. The slice of a exemplified coral sand particle with intraparticle voids is represented as coarse particle with particle–fluid mesh size ratio greater than 8. The fluid–particle interaction for the coarse particle is evaluated by the resolved scheme. Meanwhile, the red fine particle with particle–fluid mesh size ratio between 1/3 and 8 employs the semi-resolved scheme. The hybrid schemes can adaptively select the most suitable resolution scheme for fluid–particle interaction based on the particle–fluid size ratio. The implementation of hybrid SDF-CFD-DEM is utilizes the open-source code OpenFOAM and a in-house code NetDEM (Lai et al., 2022; Huang et al., 2024), developed and maintained by the third author (Lai).

3. Validation of CFD-DEM modeling of coral sand

This section presents two examples to validate the effectiveness of hybrid CDF-DEM schemes in the coral sand suffusion simulation, including the particle settling test for the resolved scheme and the Ergun's test for the semi-resolved scheme.

3.1. Particle settling test of coral sand

The particle settling test of coral sand is performed for the verification of fully resolved CFD-DEM scheme. It should be noted that although the resolved scheme has been validated with spherical particle and super-ellipsoid particle in Lai et al. (2023), its applicability to particles such as coral sand, which exhibit highly irregular apparent shapes and well-developed intraparticle voids, warrants further investigation. In this work, a 3D printing particle is employed for the particle settling test instead of using a real coral sand particle. This replacement is justified for two aspects. First, the coral sand LS particle model in the DEM is derived by down-sampling the original CT images, which results in slightly lower accuracy compared to real particles. Therefore, it is more reasonable to conduct experiments using particles that match the shape of those employed in the DEM. Second, the density of real coral sand particles is approximately 2780 kg/m^3, requiring a significant settling distance in the experiments for the particle to reach a steady velocity. This leads to an excessively large CFD fluid domain, causing unnecessary computational consumption. As illustrated in Fig. 6(a), the 3D printing coral sand particle is created using additive manufacturing to replicate the shape of the LS particle in CFD-DEM, with an equivalent particle size of 0.015 m and a density of 1200 kg/m^3. The particle is printed using resin material with a high-resolution printer (i.e., 100 μm layer thickness). The shape fidelity between the physical print and the digital LS model is verified using 3D scanning, ensuring the maximum deviation is below 0.3 mm. The particle is initially positioned 0.02 m above the bottom of the box container, which has a base of 0.05-by-0.05 m. The CFD-DEM simulations and laboratory tests are conducted with identical setups. In the simulation, the particle–fluid mesh size ratio is 30 for considering the intraparticle voids. Fig. 6(b) shows the evolution of particle settling velocity. Notably, the experimental results of particle settling velocity are based on the average of five laboratory tests, aimed at mitigating measurement errors. The findings showcase a good agreement between the simulation and laboratory tests, validating the effectiveness of the fully resolved SDF-CFD-DEM in simulating the settling of coral sand particles.

3.2. Ergun's test

The Ergun's test is employed to validate the semi-resolved CFD-DEM scheme. As depicted in Fig. 7(a), approximately 3380 spherical particles with a diameter of 0.01 m are packed into a cubic container with a base of 0.15-by-0.15 m, forming a particle bed with a height of about 0.155 m. The fluid domain extends over the particle bed with a height of 0.6 m. The bottom of the fluid domain is a velocity inlet, and the top is an outlet with zero pressure. Fig. 7(b) illustrates the pressure drop across the particle bed for different inlet velocities in the Ergun's test. Three particle–fluid mesh size ratios (i.e., 1, 3, and 6) are used in the CFD-DEM simulations. The simulation results are in good agreement with the analytical solution, which demonstrates the applicability of the semi-resolved scheme to moderately fine particles.

4. Numerical model

4.1. DEM sample preparation

Coral sand, commonly found in coastal regions, is characterized by its highly irregular and angular particle shape, which makes it more susceptible to breakage at sharp edges (Peng et al., 2022). This breakage process generates finer particles, forming a gap-graded particle size distribution (PSD) that increases the susceptibility to suffusion (Ding et al., 2024). To investigate the suffusion process in coral sand, a gap-graded coral sand sample is prepared using the SDF-DEM approach. The particle size distribution of the sample used in the simulations is shown in Fig. 8. The sample consists of both coarse and fine particles, with the coarse particles having a diameter of approximately 15 mm, while the fine particles range from 1.5 mm to 3.0 mm in diameter. The coarse particles are approximately five to ten times larger than the fine particles, with fine particles constituting 30% of the total mass. In addition, several commonly assessment criteria are applied in this study to evaluate the internal stability of the gap-graded coral sand sample (Ke and Takahashi, 2014b; Mehdizadeh et al., 2021). The evaluation results are summarized in Table 1. The results indicate that the coral sand sample is potentially unstable and vulnerable to internal erosion under seepage.

The process of generating the DEM sample is illustrated in Fig. 9. The DEM sample consists of approximately 3900 fine particles and 50 coarse particles, which are inserted into the top part of a box container. Meanwhile, the particles are allowed to settle down under gravity and reach equilibrium. The coarse and fine particles are dropped alternately to promote a uniform distribution of the final packing, as shown in Fig. 9a. The coarse particles represent the coral sand with intraparticle voids, which are modeled by the LS particle model. The fine particles are modeled as sphere particle model for simplicity. Then, the sample

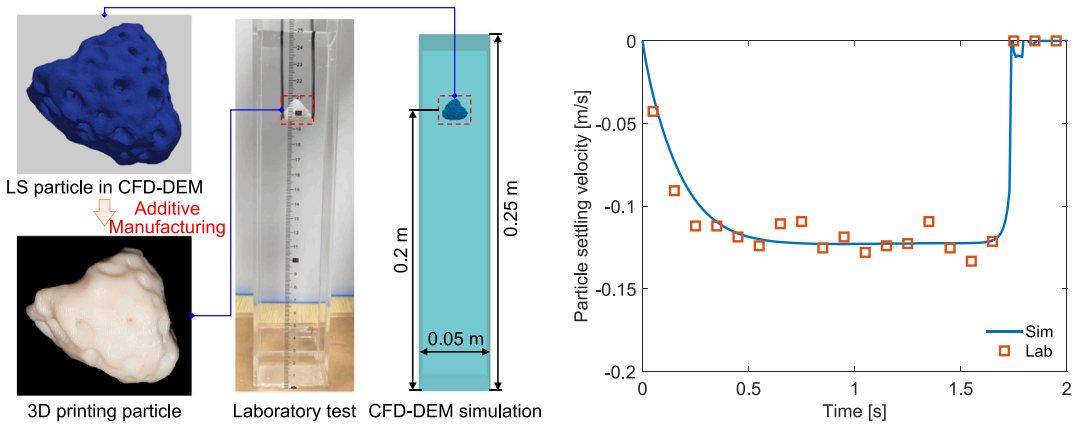

Fig. 6. Laboratory test and CFD-DEM simulation for coral sand particle settling test: (a) model setup, and (b) evolution of particle settling velocity.

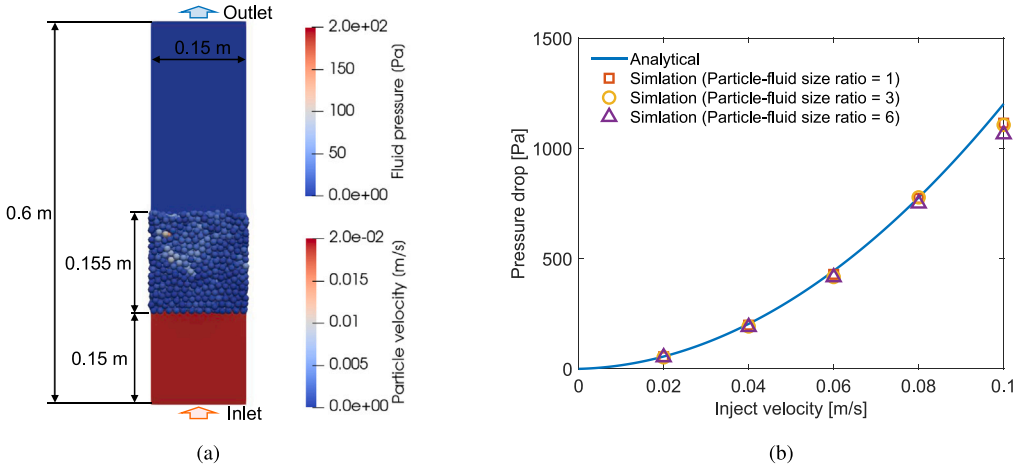

Fig. 7. Ergun's test: (a) model setup, and (b) evolution of pressure drop.

Table 1
Summary of internal stability assessment results.

Criterion	Condition of internally stable soil	Values	Internal stability
Kézdi (1979)	$(D_{15}/d_{85})_{max} \leq 4$: stable	5.0	Unstable
Kenney and Lau (1985)	$(H/F)_{min} \geq 1$: stable	0	Unstable
Mao (2005)	$4F_c(1-n) \geq 1$: stable	0.54	Unstable

Note: D_{15c} is particle size at 15% mass passing in the coarse fraction; d_{85f} is particle size at 85% mass passing in the fine fraction; H is mass fraction between grain size d and $4d$; F is mass fraction at grain size d; n is porosity.

undergoes an isotropic compression with a pressure of 50 kPa. The isotropic compression controls the relative density of the DEM sample, which is a critical factor affecting the internal stability of the packing and the susceptibility of fine particles to suffusion (Ahmadi et al., 2020). Higher relative density generally enhances packing stability, reducing the mobility of fine particles under hydraulic loading. After compression, the particle assembly forms a 0.06-by-0.06-by-0.06 m cubic sample for subsequent CFD-DEM simulations, as shown in Fig. 9b, which denotes the benchmark sample. To further investigate the effects of intraparticle voids and particle shape on the suffusion process, two additional modifications are made to the benchmark DEM sample. In Fig. 9c, the coarse particles in the benchmark DEM sample are replaced with coral sand particles represented by the SH particle model, which accounts for the apparent shape of the coral sand while deliberately removing intraparticle voids. In Fig. 9d, the fine particles in the benchmark DEM sample are replaced with irregular particles, which more closely mimic the angular shapes of natural particles. Importantly, these modifications are performed without altering the positions of the particles within the sample, as can be observed by comparing Fig. 9c and d with Fig. 9b. After the particle replacements, the contact forces within the assembly are adjusted, necessitating a brief simulation run for the sample to reach static equilibrium. Due to the pre-existing compression of the sample, particle rearrangement during this process is minimal, ensuring that the overall particle distribution remains consistent. Consequently, any differences in the simulation results can be attributed to changes in intraparticle voids and particle shape, rather than variations in the initial packing structure.

4.2. CFD-DEM simulations in suffusion process

The suffusion process of coral sand is simulated using a hybrid CFD-DEM model, as depicted Fig. 10. The DEM domain consists of a cubic sample with dimensions of 0.06 m on each side, prepared as illustrated in Fig. 9. The original bottom rigid wall of the DEM sample is replaced

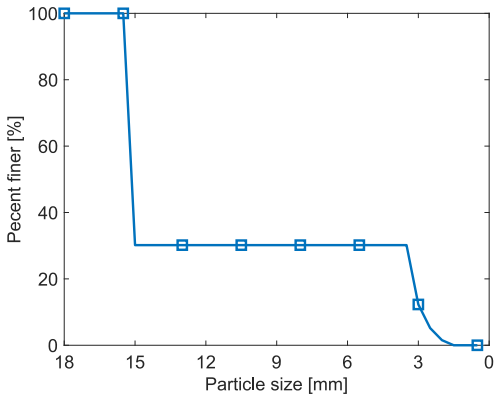

Fig. 8. Particle size distribution in the numerical simulation.

Table 2
Model parameters in CFD-DEM simulations.

Domain	Properties	Values
CFD	Domain size	0.06 m × 0.06 m × 0.064 m
	Discretization	120 × 120 × 128 cells
	Density	1000 kg/m^3
	Viscosity	1.0 × 10^{-6} m^2/s
	Timestep	adaptive
DEM	Number of coarse & fine particles	4950
	Particle density	2780 kg/m^3
	Contact normal & tangential stiffness	2.0 × 10^5, 1.0 × 10^5 N/m
	Contact friction coefficient	0.7
	Contact damping coefficient	0.3
	Timestep	2.0 × 10^{-6} s

with a filter wall featuring a hole size of 0.006 × 0.006 m, allowing fine particles to pass through while retaining coarse particles to replicate the suffusion process. The surrounding CFD domain is slightly larger, with dimensions of 0.06 × 0.06 × 0.064 m, and is discretized into a high-resolution mesh of 120 × 120 × 128 cells. The top boundary of the CFD domain is defined as a velocity inlet with a constant flow velocity of u = 0.1 m/s, while the bottom boundary is set as a zero-pressure outlet. Slip boundary conditions are imposed on the lateral walls to reduce computational complexity while preserving the realism of the flow simulation. The hybrid resolved and semi-resolved scheme is adopted to simulate the fluid–particle interactions in coral sand suffusion. For coarse particles, the particle–fluid mesh size ratio is approximately 30, allowing the flow field around these particles to be fully resolved using the resolved SDF-CFD-DEM approach. In contrast, for fine particles, the particle–fluid mesh size ratio ranges between 3 and 6, where a semi-resolved scheme is employed. This hybrid approach ensures computational efficiency while accurately capturing the flow fields both interparitcle and intraparticle coral sand particles.

The CFD-DEM model parameters are summarized in Table 2, with the parameters for coral sand adopted from Huang et al. (2023). The contact stiffness values are comparable to those previously reported by Xiong et al. (2023a).

5. Results and analysis

5.1. Effect of intraparticle voids on suffusion

To investigate the effect of intraparticle voids in coral sand on its suffusion behavior, the LS and SH particle models (see Fig. 9b and c) are employed to represent coarse particles with and without intraparticle voids, respectively. Fig. 11 illustrates the percentage of eroded particle mass (i.e., the mass ratio of the eroded fine particles to the initial fine particles) over time for coral sand with and without intraparticle voids. The results reveal a rapid initial increase in erosion, followed by a gradual stabilization, which aligns with the findings reported by Xiong et al. (2023a). Notably, the SH^C-Sphere^F sample exhibits a higher erosion percentage than the LS^C-Sphere^F, with the disparity becoming more pronounced after approximately 0.6 s. This indicates that the intraparticle voids in coral sand decrease fine particle erosion. This can be attributed to the special microstructural characteristics of coral sand particles. Specifically, intraparticle voids serve as traps for fine particles, preventing their movement induced by the fluid flow. This trapping mechanism effectively reduces the passability of fine particles. In contrast, in SH^C-Sphere^F sample, the absence of the trapping mechanism allows fine particles to be more susceptible to migration, leading to higher eroded particle mass.

To further investigate the mechanism of fine particles trapped by intraparticle voids in coral sand, Fig. 12 provides a detailed visualization of a representative coarse particle from the LS^C-Sphere^F sample after the suffusion process. The zoom-in view of the selected coarse coral sand particle along with its surrounding fine particles is shown in Fig. 12(b). By rotating to an optimal view, as illustrated in Fig. 12(c), it can be observed that two fine particles (depicted in green) are trapped within the intraparticle voids. In addition, the inside view by clipping in Fig. 12(d) further reveals that a fine particle (shown in yellow) has entered the intraparticle voids in coral sand. In contrast, Fig. 12(e) shows the similar coarse particle from the SH^C-Sphere^F sample, where the absence of intraparticle voids precludes such trapping. These observations demonstrate the capacity of intraparticle voids to trap fines. Therefore, the migratability of fine particles is reduced, which contributing to the lower eroded mass observed in coral sand with intraparticle voids.

Fig. 13 presents the evolution of the fine particles distribution in the suffusion process. The DEM sample is divided into three layers along its height: bottom, middle, and top, as shown in Fig. 13(b). The variation in the number of fine particles within each layer over time is presented in Fig. 13(a). For both LS^C-Sphere^F and SH^C-Sphere^F samples, the erosion of fine particles primarily occurs in the bottom layer, followed by the top layer, while the middle layer exhibits relatively stable fine particle content. This may be due to the proximity of the bottom layer to the outlet, making fine particles more susceptible to erosion. As suffusion progresses, the fine particles in the middle layer move downward, reducing their content. However, the fine particles from the top layer replenish the middle layer, thus maintaining a relatively stable fine particle content throughout the process. A notable distinction between the two samples lies in the number of fine particles in the top layer. The top layer of the LS^C-Sphere^F sample retains more fine particles than that of the SH^C-Sphere^F sample after suffusion. It can be caused by the trapping effect of intraparticle voids, which makes long distance transportation of the particles more difficult. The distinction is further supported by the cumulative distribution of particle migration distances for the top layer fines, as shown in Fig. 13(c). A larger fraction of fine particles in the LS^C-Sphere^F sample exhibit smaller displacements compared to the SH^C-Sphere^F sample, and the mean migration distance of top layer fines in LS^C-Sphere^F is also smaller. These observations quantitatively confirm that the intraparticle voids hinder long distance transport of fine particles, enhancing retention of fines.

The dynamic behavior of fine particles under fluid flow significantly affects the extent of erosion during the suffusion process. To explore this further, Fig. 14 provides insight into the movement patterns of fine particles by tracking their trajectories and analyzing their velocity evolution. In Fig. 14(a), the identified fine particles exhibit two primary outcomes: some are eventually eroded and transported out of the system (P_4, P_5, P_6), while others are retained in the coarse granular media region, leading to clogging (P_1, P_2, P_3). Fine particles with very close initial positions (e.g., P_2 v.s. P_6, or P_3 v.s. P_4) can also exhibit entirely different behaviors (eroding or clogging) after suffusion. The velocity evolution curves in Fig. 14(b) further reveal the dynamic characteristics of fine particles motion. Even among clogging fine particles,

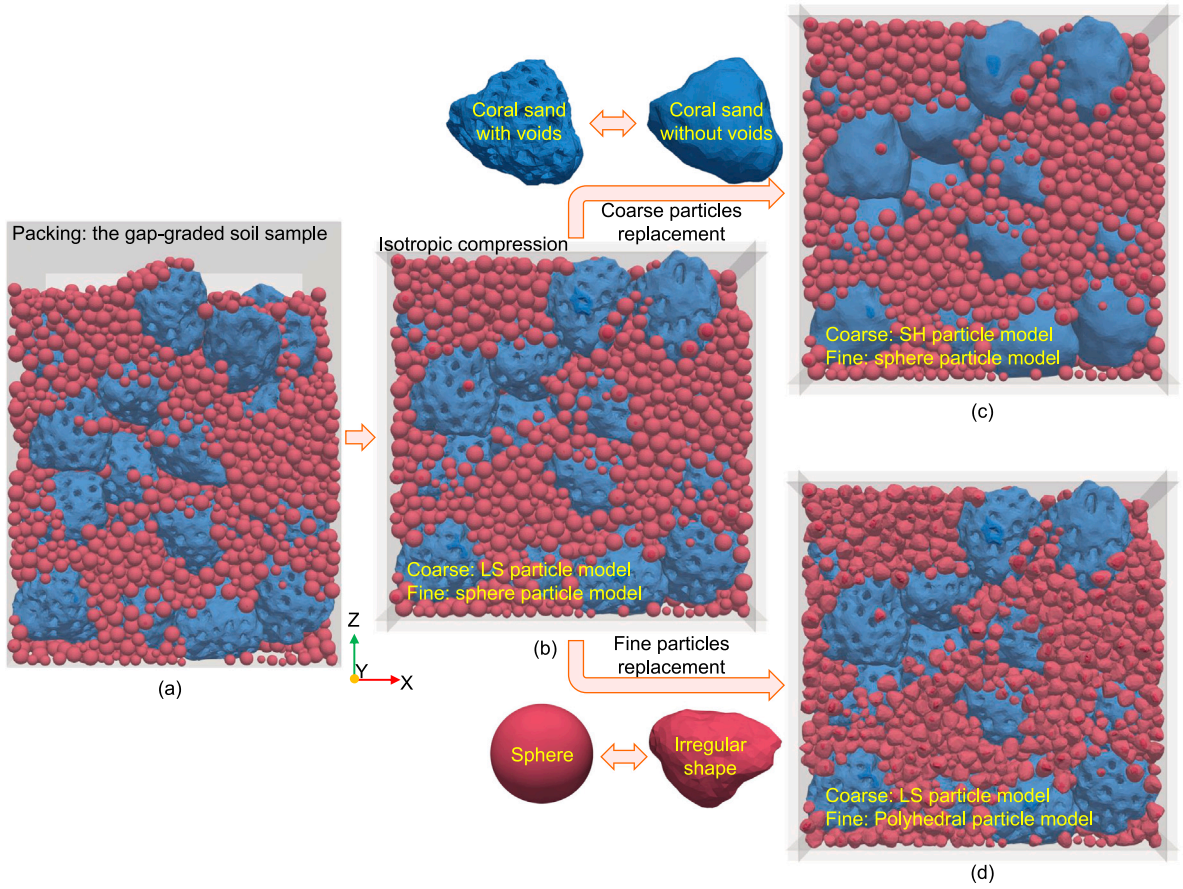

Fig. 9. Model setup of the gap-graded coral sand DEM sample.

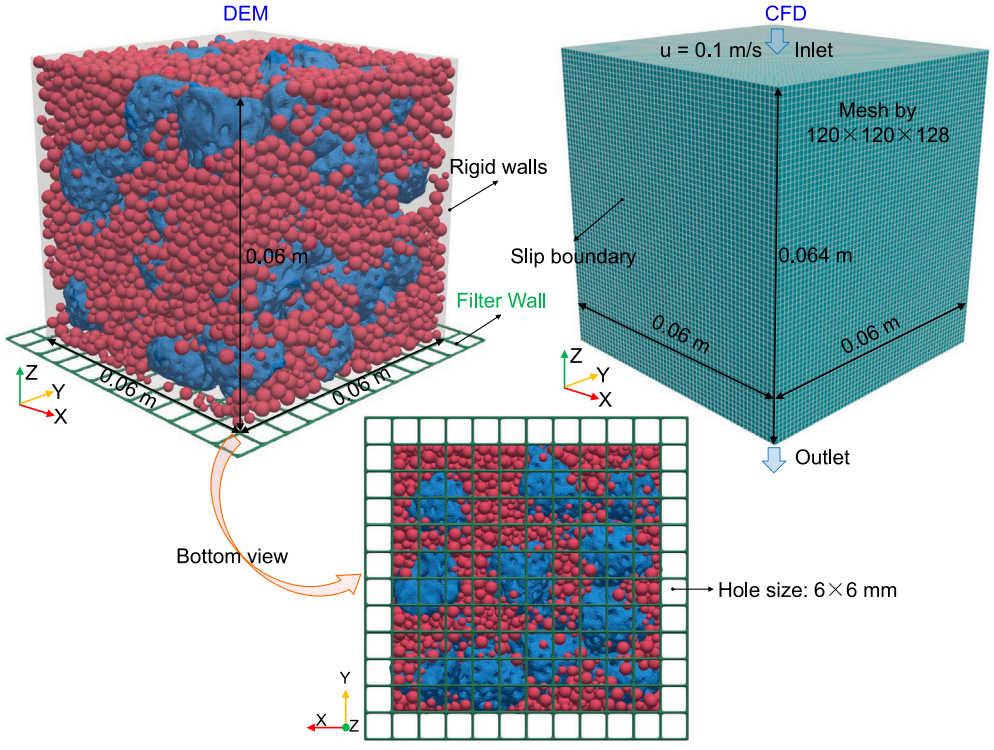

Fig. 10. Illustration of suffusion numerical model for coral sand using CFD-DEM.

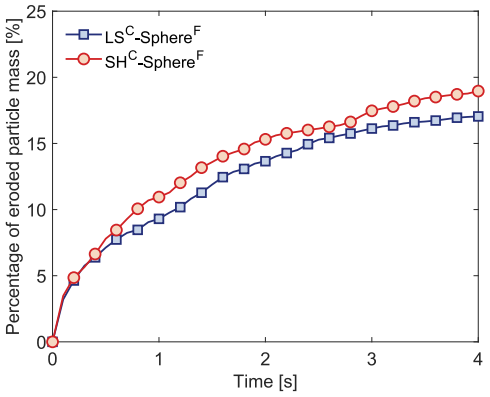

Fig. 11. Percentage of eroded particle mass for coral sand with and without intraparticle voids during the suffusion simulation. LS^C-Sphere^F indicates that the coarse particles are modeled by LS particle model, while the fine particles are represented as sphere particle model. Note that the data presented is based on a single, deterministic CFD-DEM simulation run for each condition.

distinct movement patterns can be observed. For instance, P_1 initially accelerates under fluid forces, then undergoes sudden deceleration and temporary clogging before resuming motion, exhibiting an intermittent unclogging-clogging cycle. P_2 experiences multiple velocity fluctuations before clogging. In contrast, P_3 remains clogged for the first 2 s, then suddenly accelerates as the surrounding fine particles are displaced. P_3 migrates downward before eventually becoming trapped again. Additionally, the velocity curve of a typical eroding fine particle (P_4) is also plotted in Fig. 14(b). During the unclogging process, the particle velocity of P_4 first exhibits fluctuations and then rises rapidly, indicating that the fine particle undergoes erosion and subsequently exits the sample. These variations highlight the complexity of the migration and retention behaviors of fine particles in porous media. The intermittent trapping and release of fine particles suggest that clogging is not always permanent.

Fig. 15(a) illustrates the overall hydraulic gradient evolution during the CFD-DEM simulation. The process is characterized by three distinct stages. The gradient initially reaches a sharp transient peak, signifying the maximum flow resistance caused by the initial rearrangement and temporary clogging of fine particles. This is immediately followed by a rapid, substantial decrease in hydraulic gradient, as the seepage force breaks the temporary bridges. The gradient subsequently stabilizes at a lower equilibrium value, indicating the system has reached a new, stable hydraulic configuration. The pronounced fluctuations observed throughout the main erosion phase result from the alternating local cycles of particle clogging and unclogging. Hydraulic conductivity is the critical macroscopic parameter governing the stability under seepage conditions (Chen et al., 2025). As shown in Fig. 15(b), after an initial slight drop due to temporary clogging, hydraulic conductivity undergoes a rapid and substantial increase, rising from its minimum of approximately 1.7 cm/s to a final stable value of approximately 4.4 cm/s. This more than twofold increase is the macroscopic output of the massive fine particle washout, signifying the significant reduction in flow resistance. The fluctuations observed in hydraulic conductivity during the rapid rise phase reflect the continuous opening and narrowing of flow paths driven by particle rearrangement and localized structural collapse.

To gain deeper insight into the influence of intraparticle voids on fluid flow, we visualize the intraparticle flow velocity fields in coral sand, as illustrated in Fig. 16. A coral sand particle from the LS^C-Sphere^F sample is selected, and the surrounding hexahedral fluid region is extracted to examine the localized flow behavior in detail. A slice along the center of the coral sand specimen is taken to create a cross-sectional view of both the particles and the fluid for better visualization. The slice of fluid velocity field reveals that fluid flows into the intraparticle voids of the coral sand, yet the velocity within these voids is noticeably lower than that in the interparticle spaces. This reduction in velocity can be ascribed to the restricted space within the intraparticle voids, which impose greater flow resistance and limit fluid mobility compared to the relatively open interparticle pathways. Furthermore, Fig. 17 quantifies these observations by showing the evolution of the average interparticle and intraparticle flow velocities. It should be noted that the interparticle flow refers to the movement of fluid in the spaces between coarse coral particles. The results indicate that the flow velocity within intraparticle voids remains relatively stable during the suffusion process and is significantly lower than the interparticle flow velocity. In both LS^C-Sphere^F and SH^C-Sphere^F samples, the interparticle flow velocity initially increases before gradually stabilizing.

5.2. Effect of particle shape on suffusion

Particle shape is also a key factor in governing suffusion behavior, as it affects fluid–particle interactions and particle interlocking (Liu et al., 2024; Liu and Yin, 2024). In view of this, the effects of both fine and coarse particle shapes on suffusion are evaluated through a comparative analysis of three distinct samples: LS^C-Polyhedral^F, LS^C-Sphere^F, and Sphere^C-Sphere^F. Fig. 18 presents the particle configurations before and after suffusion for these three samples. Initially, all samples exhibit a densely packed structure with fine particles filling the voids between coarse grains. The LS^C-Polyhedral^F and LS^C-Sphere^F samples maintain an identical particle arrangement to focus on the effect of the fine particle shape on suffusion. However, for the Sphere^C-Sphere^F samples, a new coarse particle configuration is generated due to the significant shape discrepancy between spherical and natural coral sand particles. This adjustment is necessary to achieve a reasonable initial packing structure, as directly replacing natural-shaped coarse particles with spheres would have resulted in unrealistic packing behavior. After suffusion, visible fines erosion can be observed in the bottom regions among the three samples. Specifically, the pronounced differences in the regions highlighted by the green dashed boxes indicate the influence of fine particle shape on suffusion. The LS^C-Sphere^F sample exhibits a greater loss of fine particles, suggesting that spherical fine particles are more susceptible to suffusion compared to irregular fine particles.

Fig. 19 shows the percentage of the eroded particle mass over time for three samples with different particle shapes. It can be observed that the sample with irregular fine particles (LS^C-Polyhedral^F) exhibits the least erosion, while the sample with spherical fine particles (LS^C-Sphere^F) shows a greater degree of suffusion. The Sphere^C-Sphere^F sample shows the highest erosion percentage. This suggests that both fine and coarse particle shapes significantly influence the suffusion process, with spherical particles exhibiting greater susceptibility to erosion. The lower erosion observed in LS^C-Polyhedral^F can be attributed to the interlocking effect of irregular particles, which enhances structural stability and reduces the mobility of fine particles. In contrast, the LS^C-Sphere^F sample exhibits higher erosion due to the relatively smooth and rounded fine particles, which are more easily transported by fluid flow. The Sphere^C-Sphere^F sample further amplifies this effect, as the spherical coarse particles provide fewer constraints on the movement of fine particles. Previous suffusion simulations of coral sand often used spherical particles for simplification, and ignored its complex morphology (Xiong et al., 2023a,b). This simplification can significantly overestimate the extent of fines erosion,resulting in approximately 2.5 times overprediction in this work. These results highlight the necessity of incorporating realistic particle morphologies to more accurately assess suffusion behavior in coral sand.

The evolution of fine particles distribution in different layers of three samples is illustrated in Fig. 20. As expected, fine particles erosion

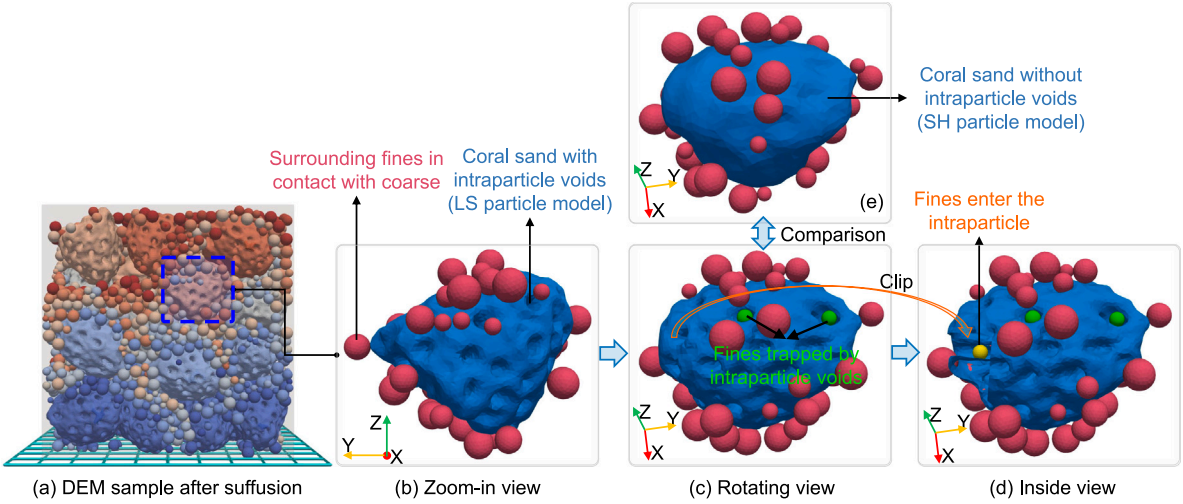

Fig. 12. Visualization of fine particles trapped by intraparticle voids in coral sand after suffusion. (For interpretation of the references to color in this figure legend, the reader is referred to the web version of this article.)

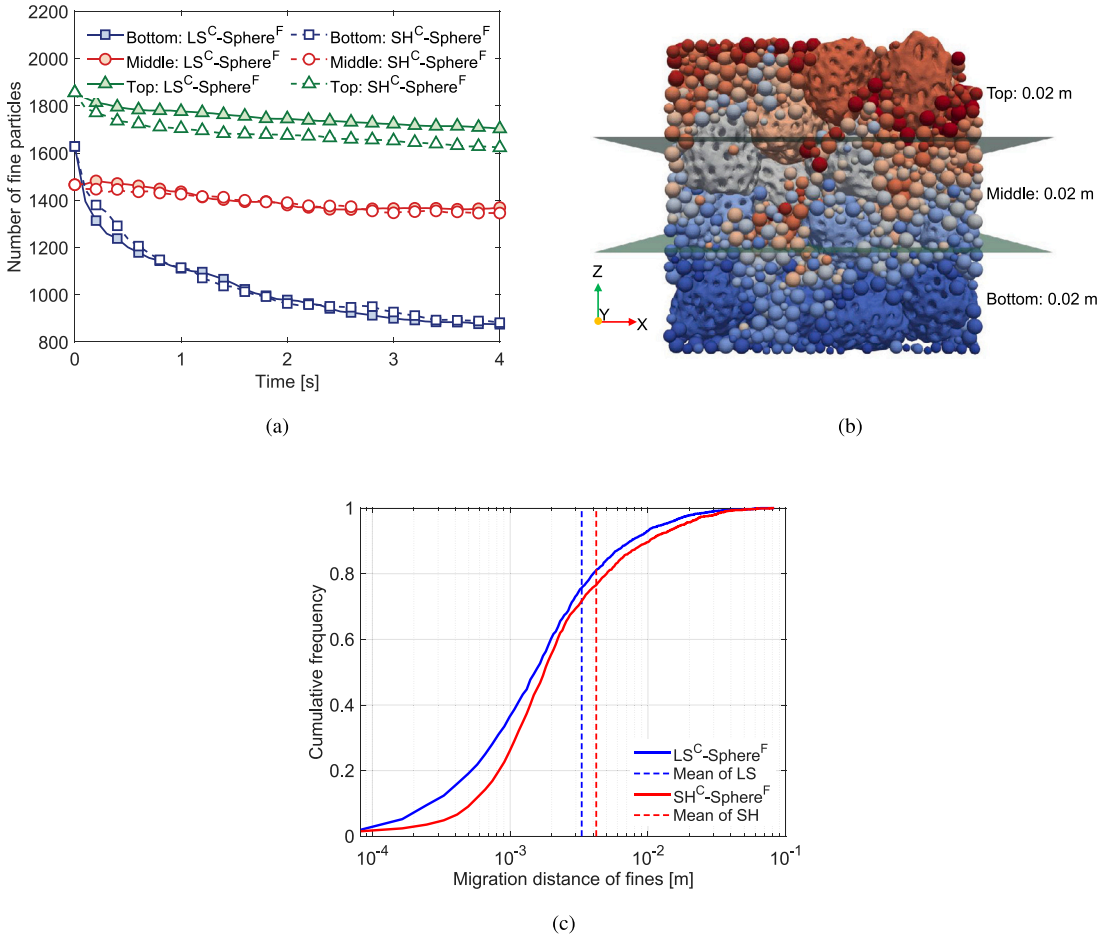

Fig. 13. Evolution of the fine particles distribution in the suffusion process: (a) temporal variation of fine particles in different layers, (b) spatial partitioning of the sample, and (d) cumulative distribution of migration distances of top layer fines.

is most pronounced in the bottom layer across all samples. In the middle and top layers, the two samples incorporating realistic coral sand particle shapes (LS^C-$Sphere^F$ and LS^C-$Polyhedral^F$) exhibit only a slight decrease in fine particle content over time, with the number of irregular fine particles remaining nearly constant. However, the $Sphere^C$-$Sphere^F$ sample shows a more noticeable reduction in fine particles, indicating that the spherical coarse particle skeleton provides more migration channels for fine particles.

Fig. 21 presents the distribution of migration distances for fine particles during the suffusion process for three samples with different particle shapes. The distribution curves of three samples exhibit an approximately exponential decay with increasing migration distance.

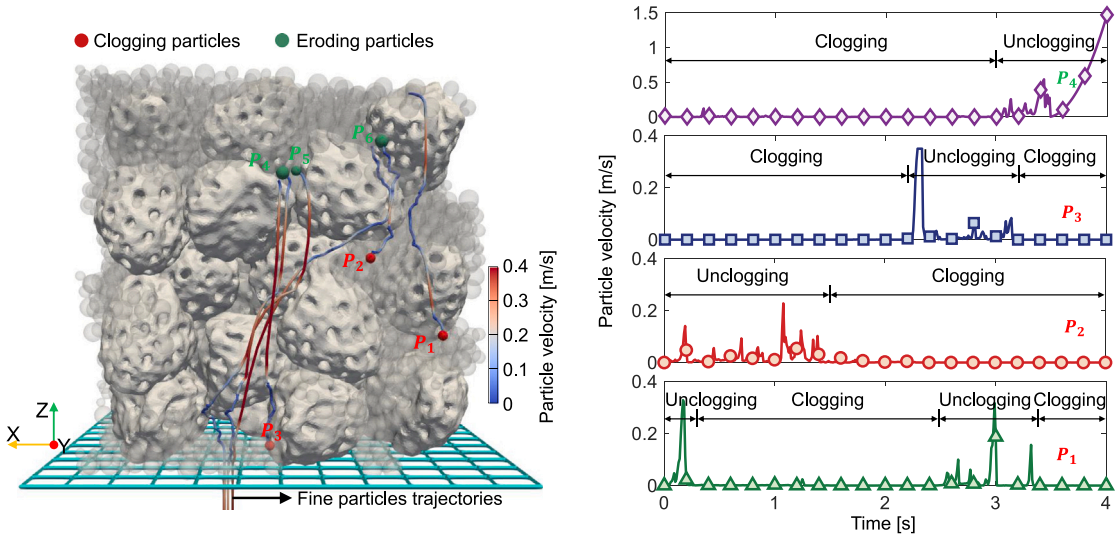

(a) (b)

Fig. 14. Illustration of (a) representative trajectories of clogging and eroding fine particles, and (b) velocity profiles of clogging and eroding fine particles over time.

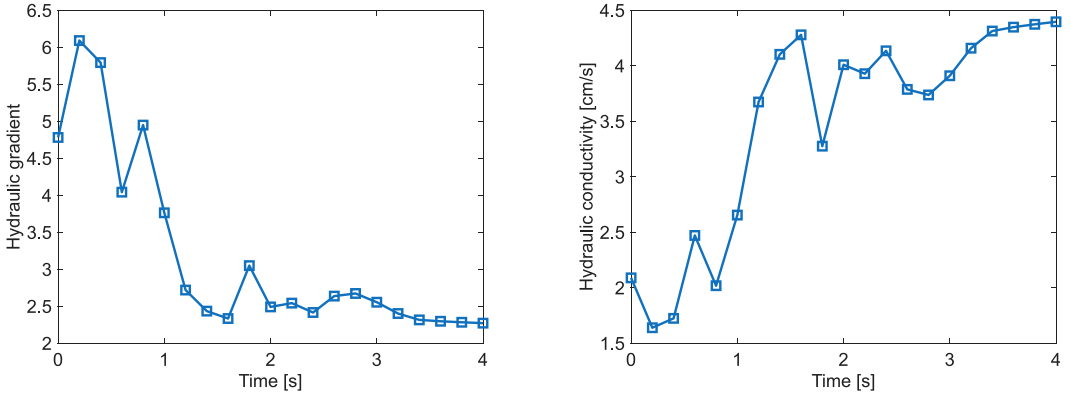

(a) (b)

Fig. 15. Evolution of (a) hydraulic gradient and (b) hydraulic conductivity during the suffusion process for LS^C-Sphere^F sample.

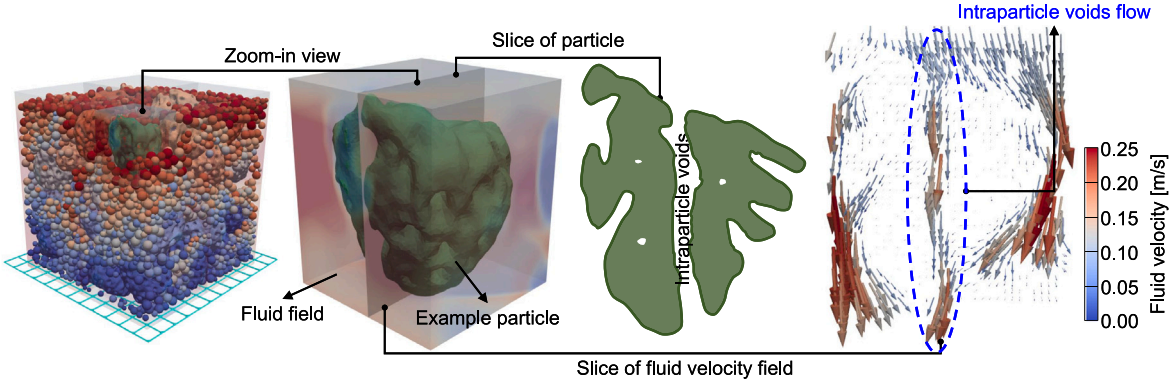

Fig. 16. Visualization of intraparticle flow velocity fields in coral sand.

It suggests that most of the fine particles migrate over short distances, while relatively few migrate over long distances. The Sphere^C-Sphere^F sample exhibits the largest number of fines capable of long distance migration. In contrast, the LS^C-Polyhedral^F sample shows a rapid decrease in the number of migrating fines with increasing distance, implying a strong suppression of particle migration. This behavior can be attributed to particle interlocking, which arises from the angular geometries of irregular particles. In the LS^C-Polyhedral^F sample, the irregular fine particles are more prone to mechanical engagement with the surrounding coarse particles, increasing geometrical constraints

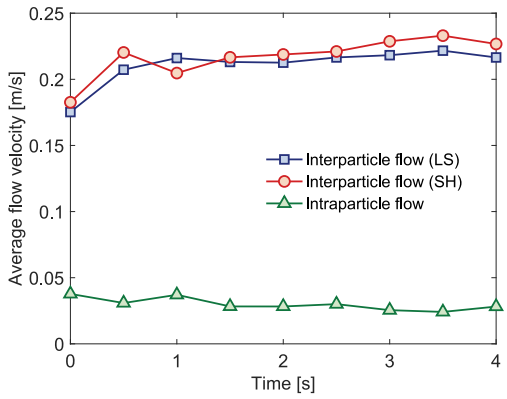

Fig. 17. Evolution of average interparticle and intraparticle flow velocities.

during transport. Such interlocking impedes the migration of fine particles, leading to reduced effective transport distances and enhanced retention.

5.3. Sensitivity analysis of suffusion to flow velocity and direction

In addition to the morphological characteristics of coral sand, the suffusion process is significantly influenced by the fluid flow velocity and direction (Liu et al., 2020; Xiong et al., 2021b). To further demonstrate the capability of the proposed numerical framework, we performed sensitivity analysis of suffusion to flow velocity and direction. As illustrated in Fig. 22, a series of simulations are conducted under different inlet velocities and flow directions. In this work, three inlet velocities (i.e., u = 0.01, 0.05, 0.10 m/s) are selected, where 0.01 m/s is close to the critical erosion threshold for sandy soils (Richards and Reddy, 2012), while 0.05 and 0.10 m/s represent stronger seepage conditions commonly encountered under wave-driven marine environments. The flow directions (i.e., $\theta = 0°, 45°, 90°$) follow previous sensitivity studies on suffusion anisotropy to capture the effects of vertical, oblique, and horizontal flow (Xiong et al., 2021b). It should be noted that the flow direction is parameterized by the angle (θ) between flow direction and gravity. In the numerical setup, the flow direction is fixed along the negative z-axis, while the gravity direction is rotated to achieve different angles (Liu et al., 2024; Xiong et al., 2021b). Here, $\theta = 0°$ represents the conventional vertical downward seepage (aligned with gravity), $\theta = 90°$ corresponds to horizontal flow (perpendicular to gravity). For simulations exploring the effect of inlet flow velocity, the flow direction remains aligned with gravity. Conversely, for those examining the effect of flow direction, the inlet velocity is fixed at 0.1 m/s.

The percentage of eroded particle mass under different inlet flow velocities and flow directions is depicted in Fig. 23. In Fig. 23(a), the overall trend shows that higher inlet velocities lead to increased fine particle erosion. Initially, the erosion percentage is rapid for all cases, followed by a gradual stabilization as the suffusion process progresses. Interestingly, while the lowest velocity case (u = 0.01 m/s) initially exhibits a slightly higher erosion percentage, it is eventually surpassed by the higher velocity cases (u = 0.05 m/s and u = 0.10 m/s). This can be explained by the fact that higher velocities generate larger fluid–particle interaction forces. These forces lead to an increase in contact forces, which temporarily stabilizes the fine particles and inhibits their migration at the initial stage. As the suffusion process continues, the particles are rearranged and gradually loosened, which leads to easier separation and transportation of fine particles. As a result, the erosion percentage in the higher velocity case will increase over time and eventually exceed that in the lower velocity case. As shown in Fig. 23(b), the erosion percentage decreases with the angle θ between the flow direction and gravity increases. When $\theta = 0°$ (flow aligned with gravity), the downward fluid force enhances particle migration, resulting in the highest erosion percentage. In contrast, as θ increases to 45° and further to 90°, the variation in gravity direction prevents fine particles from migrating along the flow direction, increasing the migration distance and reducing the erosion percentage. This numerical observation is consistent with recent experimental studies that have revealed the significant influence of non-vertical flow paths on internal erosion behavior. The important experimental studies by Chen et al. (2021, 2024), utilizing specialized permeameters, confirmed that suffusion exhibits clear anisotropy in soils. Their findings experimentally validate the general premise that the flow direction relative to the principal stress or gravity vector is a critical factor governing the efficiency of particle migration and the overall erosion process. Our CFD-DEM simulation quantitatively supports this understanding by demonstrating that the alignment of the seepage vector with gravity maximizes particle expulsion, while deviation promotes particle trapping and reduces total mass loss.

Furthermore, the distribution of fine particles after suffusion is shown in Fig. 24. As the inlet velocity increased, the number of fine particles decreases slightly in all layers, with the most significant decrease in the top layer. This is due to the fact that the top layer is close to the inlet and the higher flow velocity enhances the mobility of the fine particles and promotes their downward migration. In Fig. 24(b), as θ increases, the overall distribution remains consistent in the middle and top layers, but a noticeable increase in fine particle retention is observed in the bottom layer. This indicates that as the flow deviates from the gravity direction, the transport efficiency of fine particles decreases, leading to an increase in the accumulation of fine particles in the coarse granular media region. The inclined flow directions leads to more complex fine particle trajectories, thereby increasing the likelihood of fine particles retention within the sample.

Fig. 25 illustrates the evolution of fluid–particle interaction forces under different inlet flow velocities and flow directions. The results show that coarse particles experience greater fluid–particle interaction forces than fine particles, which is mainly due to the linear relationship of the interaction forces on particle volume. Moreover, the interaction force increases with flow velocity, suggesting that higher velocities intensify the momentum exchange between the fluid and particles. In contrast, the effect of flow direction on the interaction force is minimal, likely because it does not induce significant variations in the average fluid velocity within the sample.

The contact fabric of soil has been shown to significantly influence its micromechanical behavior (Guo and Zhao, 2013; Song et al., 2024). Therefore, the evolution of anisotropy in contact normal orientation during the suffusion process is investigated and presented in Fig. 26. In Fig. 26(a), the degree of anisotropy in contact normal orientation under different inlet flow velocities follows a similar trend as it initially decreases rapidly and then gradually stabilizes. The primary distinction lies in the magnitude of fluctuations, with higher inlet velocities resulting in more pronounced variations in anisotropy. This is due to stronger fluid–particle interactions at higher velocities, which induce more frequent particle rearrangements and transient force chain reconfigurations. As a result, the contact network becomes more dynamic, leading to greater fluctuations in anisotropy before stabilizing. As depicted in Fig. 26(b), the anisotropy in contact normal orientation increases with the angle between the flow direction and gravity during the suffusion process. This suggests that as the flow direction deviates further from gravity, the fluid exerts a stronger shear effect on the particle assembly, leading to a more anisotropic contact structure. At larger flow angles, the suffusion process likely results in more asymmetric erosion patterns and heterogeneous contact force distributions, which enhance the anisotropy in contact normal orientation.

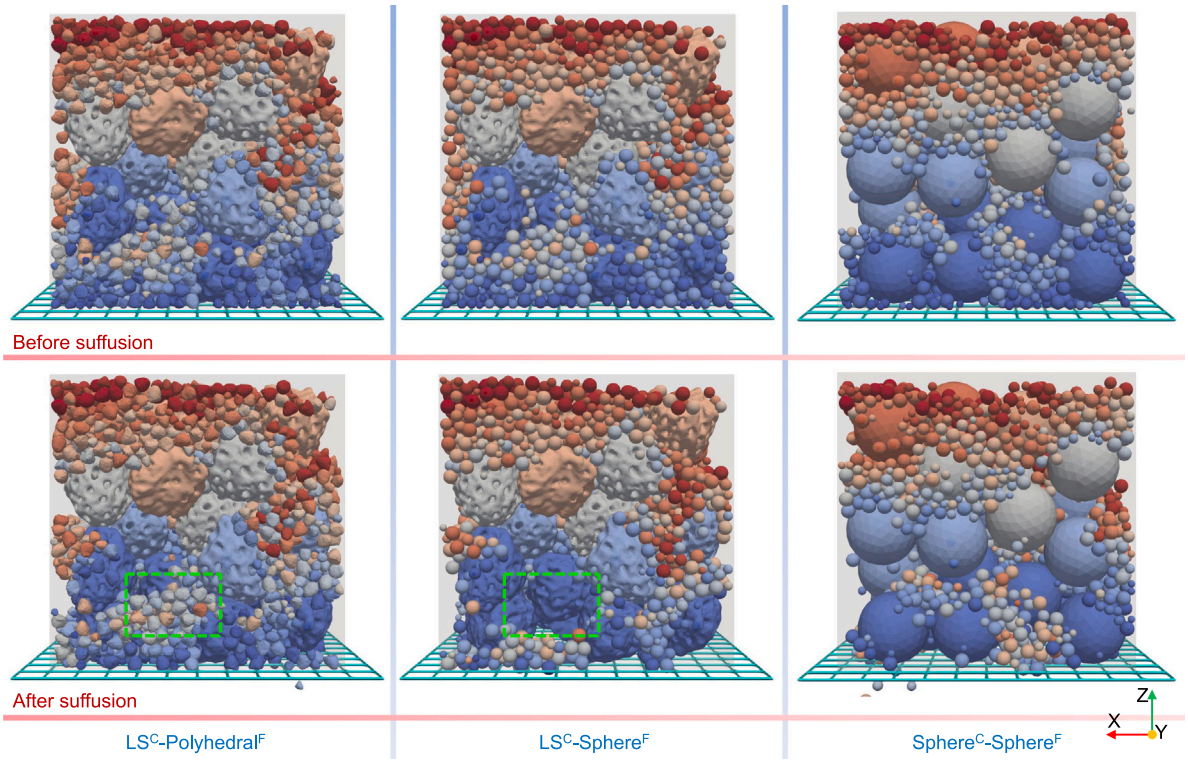

Fig. 18. Snapshots of particle configurations before and after suffusion for different particle shapes. (For interpretation of the references to color in this figure legend, the reader is referred to the web version of this article.)

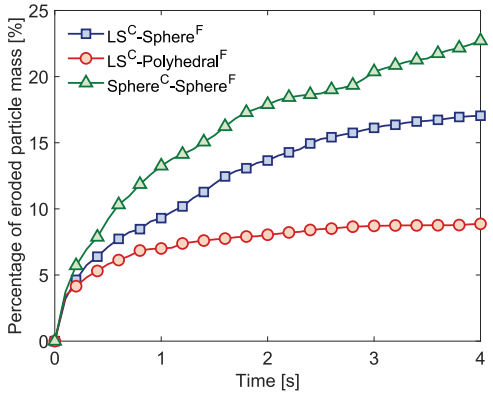

Fig. 19. Percentage of eroded particle mass for different particle shapes.

6. Discussion

The accurate prediction of seepage stability in coral sand requires a profound understanding of the complex interaction between fluid flow and particle morphology. This study reveals that the internal stability of coral sand is governed by the synergistic effects of interparticle interlocking and intraparticle trapping. High-fidelity morphological characterization is necessary to capture these micromechanical features accurately. Our results show that irregular particle shapes significantly strengthen interparticle interlocking. This irregularity also increases the tortuosity of pore channels. Such geometric constraints effectively restrict the migration process of fine particles. These findings align with existing experimental studies. For instance, Slangen and Fannin (2017) observed higher erosion resistance in angular particles compared to spherical glass beads under identical gradations. Furthermore, Maroof et al. (2021) concluded from systematic tests that grains with lower regularity offer greater resistance to suffusion. Their study showed that an increase in sphericity and roundness leads to higher mass loss and vertical strain. These consistent observations demonstrate that conventional spherical models overlook the stabilizing effect of shape interlocking. Consequently, simplified models inevitably overestimate the erosion of fine particles. This discrepancy suggests that current empirical erosion laws require the integration of particle shape parameters to improve quantitative predictions of soil loss (Nguyen et al., 2016).

Beyond apparent particle morphology, the explicit representation of intraparticle voids introduces a trapping mechanism that influences fines migration. It is worth noting that these findings differ from those reported in Wang et al. (2022b), which observed higher erosion in coral sand with intraparticle voids. This discrepancy arises from differences in the representation of coarse particle morphology. In Wang et al. (2022b), the intraparticle flow field is modeled using the dynamic fluid mesh (DFM) approach, while the solid phase of coral sand particles is represented by sphere particle model in the DEM. As a result, the complex morphology and intraparticle voids of real coral sand are not explicitly modeled, limiting the ability of coarse particles to trap and retain fine particles. Consequently, the presence of intraparticle flow fields primarily enhances local fluid flow, leading to increased fine particles erosion. However, the impact of intraparticle voids on fine particles erosion also depends on the size ratio between fine particles and intraparticle voids. When the fine particles are significantly smaller than the voids, they may pass through rather than being retained, potentially leading to increased erosion. Furthermore, this phenomenon can be conceptually modeled as a size-dependent filtration process where the fines-to-void size ratio dictates the fate of the migrating fines. For instance, a small ratio tends towards penetration, while a near-critical ratio favors clogging and retention at the void entrance. A feasible way to quantitatively examine this transition is to conduct simplified DEM-CFD simulations of fine particles passing through a single porous coral particle under seepage flow. This approach will allow us to evaluate the critical thresholds for retention and penetration by systematically adjusting the size ratio, and will constitute a major

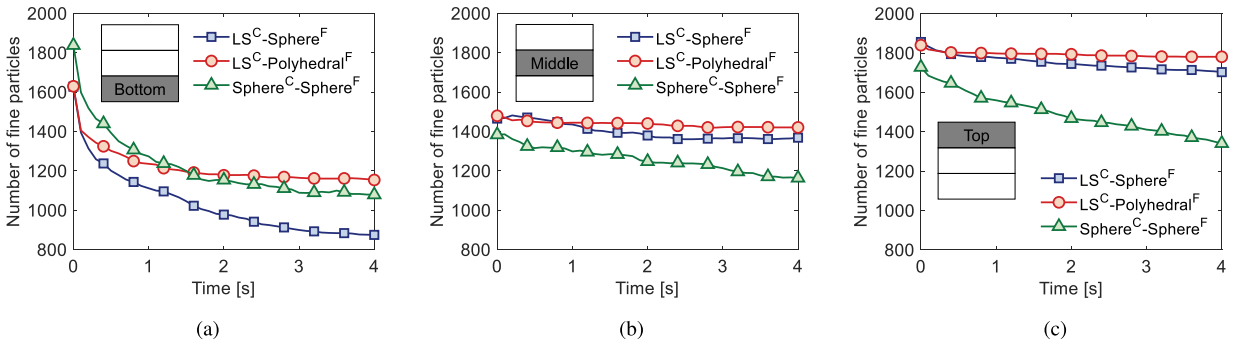

Fig. 20. Evolution of fine particles distribution in (a) bottom, (b) middle, and (c) top layer of the samples with different particle shapes during the suffusion process.

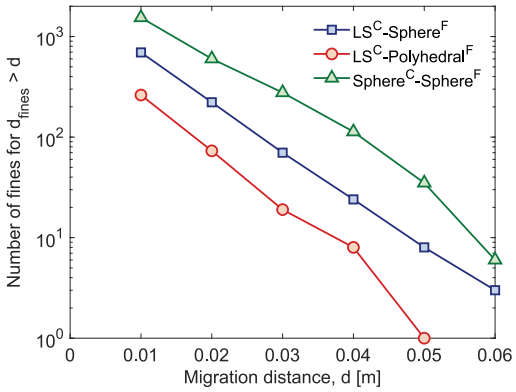

Fig. 21. Migration distance distribution of fine particles during suffusion for different particle shapes. Note that the migration distance (d) of fine particles is defined as the total length of the particle trajectory during suffusion, and the vertical axis indicates the number of fine particles with migration distance exceeding a given threshold.

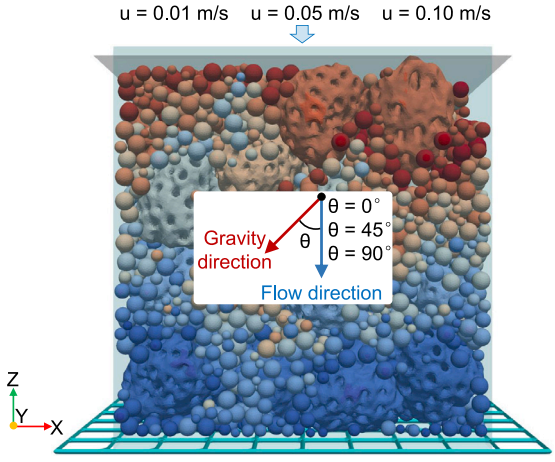

Fig. 22. Illustration of suffusion sample under varying inlet flow velocities and flow directions.

focus of our future work to fully reveal the mechanics of fines migration within intraparticle voids.

Building upon the insights gained from high-fidelity morphological modeling, future investigations will incorporate particle breakage mechanics into the hybrid SDF-CFD-DEM framework to capture the intrinsic crushability of coral sand. In marine environments, the erosion of fine particles inevitably leads to a redistribution of skeleton stresses (Shahnazari and Rezvani, 2013). This process can trigger the crushing of coarse grains at their contact points due to localized stress concentrations. The crushability of coral sand fundamentally alters its hydraulic conductivity (Yan et al., 2025). The interaction between breakage and erosion likely creates a dynamic feedback loop. Particle breakage generates new fine fragments that provide a continuous source for further suffusion. Simultaneously, the loss of these fines reduces the lateral support of the grain skeleton, potentially promoting additional crushing. To capture these complex dynamics, one promising approach is the implementation of a level set splitting technique (Harmon et al., 2020). By utilizing fracture surfaces defined by level set functions, this method allows for the explicit description of arbitrary shapes for both particles and fracture surfaces. Capturing this coupling mechanism is critical for achieving high-fidelity predictive capabilities. Such advancements are essential for accurately assessing the long-term settlement and potential failure of offshore foundations under extreme cyclic loading.

7. Conclusions

This work presents a numerical modeling framework for suffusion in coral sand, integrating a hybrid resolved and semi-resolved SDF-CFD-DEM approach to accurately capture fluid–particle interactions, irregular shapes, and intraparticle voids of coral sand particles. In this framework, the level set (LS) particle model is employed to represent coral sand with intraparticle voids, and the spherical harmonics (SH) particle model is used to capture the apparent shapes of coral sand particles. The fully resolved scheme is applied to coarse particles, enabling a detailed representation of flow around complex particle geometries, while the semi-resolved scheme is adopted for fine particles, effectively reducing computational costs. The effectiveness of the hybrid CDF-DEM schemes in the coral sand suffusion simulation is validated through the particle settling test of coral sand and Ergun's test. With this modeling framework, this study systematically investigates the effects of intraparticle voids and particle shape, along with a sensitivity analysis on flow velocity and flow direction, on the suffusion process. Main findings of this work are summarized as follows:

1. Intraparticle voids of coral sand reduce suffusion by serving as effective traps for fine particles. During the suffusion process, fine particles are either obstructed at the entrances of intraparticle voids or directly transported into these internal cavities within coarse grains, where they become immobilized. This trapping mechanism interrupts their migration and reduces the fines erosion. Flow field analysis further reveals that these voids create local low-velocity zones and disrupt streamline continuity, thereby diminishing the potential for sustained particle transport.
2. Irregular particle shapes of coral sand reduce suffusion primarily through enhanced interlocking. Non-spherical fine particles exhibit restricted motion due to geometric interlocking with neighboring grains. Similarly, irregular coarse coral sand particles provide more

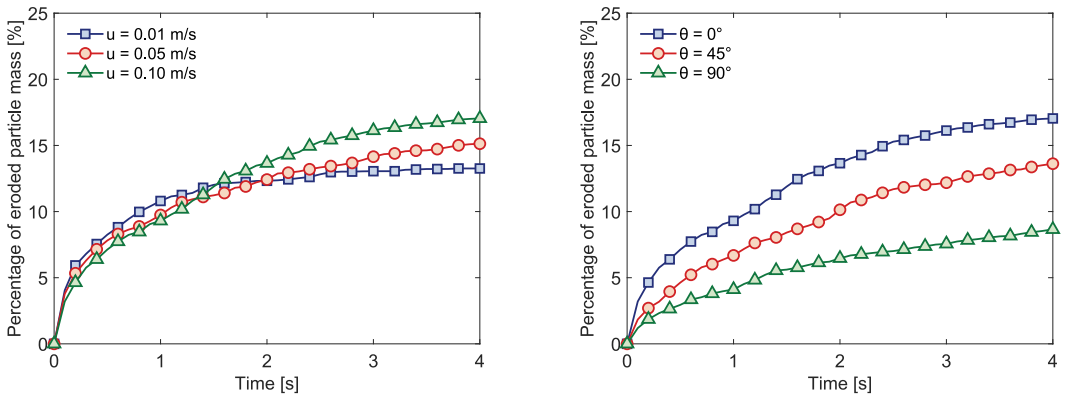

(a) (b)

Fig. 23. Percentage of eroded particle mass under different (a) inlet flow velocities and (b) flow directions.

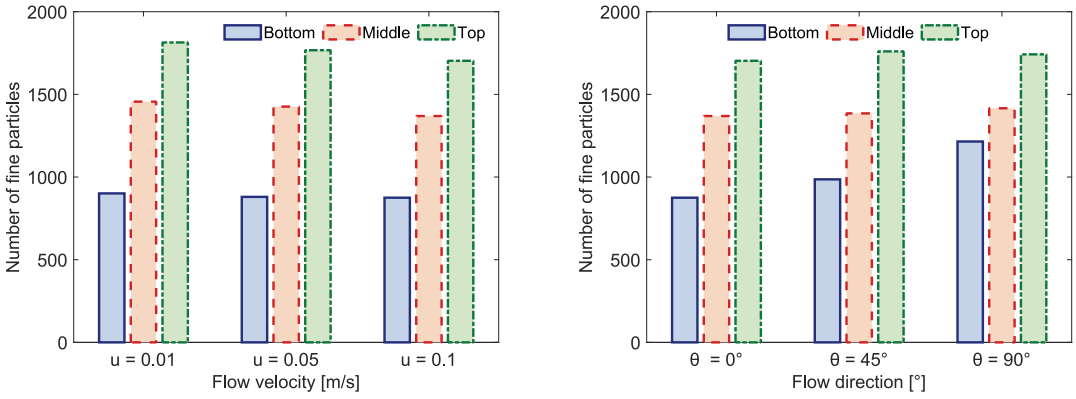

(a) (b)

Fig. 24. Distribution of fine particles after suffusion under different (a) inlet flow velocities and (b) flow directions.

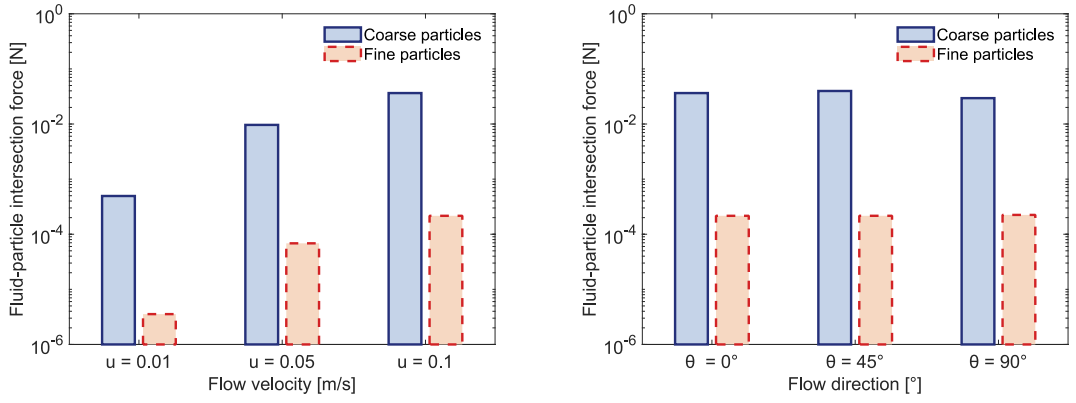

(a) (b)

Fig. 25. Evolution of average fluid–particle interaction force under different (a) inlet flow velocities and (b) flow directions.

tortuous flow paths and surface features that obstruct fine particle passage. These results demonstrate that simplified particle shapes overpredict fine particle erosion, highlighting the necessity of modeling realistic shapes.

3. Suffusion behavior in coral sand is positively correlated with inlet flow velocity and negatively correlated with flow direction deviation from gravity. Higher inlet flow velocity increases erosion by enhancing fluid–particle interaction forces and promoting fine particle migration. Flow direction significantly influences erosion pathways, with greater deviation from gravity reducing fine particle erosion. Additionally, higher velocities amplify fluctuations in contact normal anisotropy, while inclined flow directions further enhance this anisotropy.
4. Microscale analyses shows that suffusion behavior of coral sand is influenced by particle geometry and local flow structures. The trajectories of fine particles are limited by the surrounding pore structure, with irregular particle assemblies generate more tortuous and confined pathways, reducing migration distances. In addition,

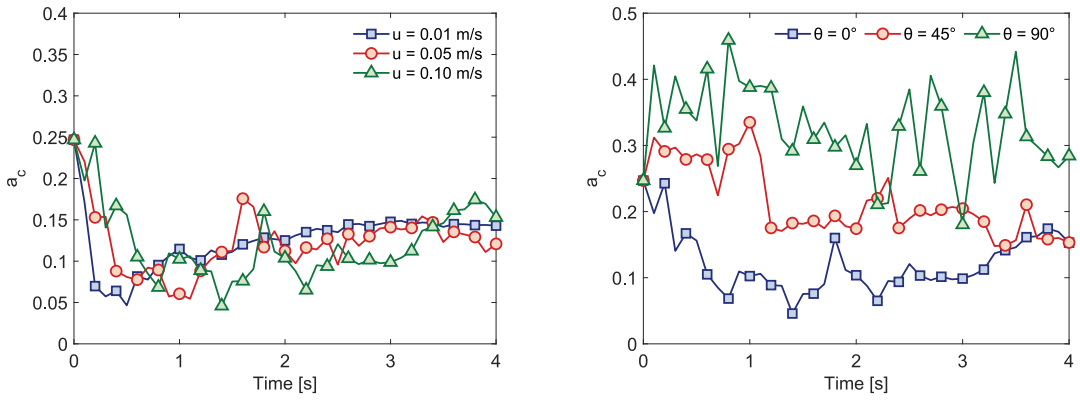

(a) (b)

Fig. 26. Evolution of the degree of anisotropy in contact normal orientation under different (a) inlet flow velocities and (b) flow directions.

while flow is present within intraparticle voids, it remains significantly slower than interparticle flow, which enhances the ability to retain fine particles.

Overall, this study advances the numerical modeling approach of suffusion in coral sand by incorporating realistic particle morphology and intraparticle voids, providing novel insights into the fundamental mechanisms governing fine particles erosion and clogging. The hybrid SDF-CFD-DEM approach enhances the predictive capability of CFD-DEM simulations for suffusion and offers valuable guidance for offshore and coastal engineering applications, particularly in evaluating the stability of coral sand under seepage conditions. However, the current work does not incorporate particle breakage, which is known to significantly influence the mechanical behavior of coral sand. The interaction between suffusion and particle breakage remains largely unexplored. In addition, the highly detailed geometric construction of coral sand leads to considerable computational cost. Integrating surrogate modeling or machine learning-based acceleration strategies presents a promising means to improve computational efficiency and enable larger scale simulations.

CRediT authorship contribution statement

Shuai Huang: Writing – original draft, Visualization, Validation, Methodology, Formal analysis, Data curation, Conceptualization. **Pei Wang:** Writing – review & editing, Supervision, Resources, Conceptualization. **Zhengshou Lai:** Writing – review & editing, Software, Methodology. **Zhen-Yu Yin:** Writing – review & editing, Resources. **Linchong Huang:** Writing – review & editing, Resources. **Changjie Xu:** Writing – review & editing, Resources.

Declaration of competing interest

The authors declare that they have no known competing financial interests or personal relationships that could have appeared to influence the work reported in this paper.

Acknowledgments

This work has been financially supported by the National Key R and D Program of China (2023YFC3009400), the National Natural Science Foundation of China (42207210, 52478428), the Research Grants Council of Hong Kong (15226322, 15220221, 15229223, 15227923), the Natural Science Foundation of Jiangxi Province, China (20242BAB26079), and the Young Science and Technology Talent Cultivation Program of Guangdong Association for Science and Technology, China (SKXRC2025003).

Data availability

Data will be made available on request.

References

Ahmadi, M., Shire, T., Mehdizadeh, A., Disfani, M., 2020. DEM modelling to assess internal stability of gap-graded assemblies of spherical particles under various relative densities, fine contents and gap ratios. Comput. Geotech. 126, 103710.
Alba, J., Audibert, J., 1999. Pile design in calcareous and carbonaceous granular materials, and historic review. In: Proceedings of the 2nd International Conference on Engineering for Calcareous Sediments. Vol. 1, AA Balkema, Rotterdam, pp. 29–44.
Andò, E., Viggiani, G., Hall, S., Desrues, J., 2013. Experimental micro-mechanics of granular media studied by X-ray tomography: recent results and challenges. Géotech. Lett. 3 (3), 142–146.
Chao, Z., Li, Z., Dong, Y., Shi, D., Zheng, J., 2024. Estimating compressive strength of coral sand aggregate concrete in marine environment by combining physical experiments and machine learning-based techniques. Ocean Eng. 308, 118320.
Chao, Z., Zhou, J., Shi, D., Zheng, J., 2025. Particle size effect on the mechanical behavior of coral sand–geogrid interfaces. Geosynth. Int. 1–17.
Chen, T., Hu, Z., Yang, Z., Zhang, Y., 2023. A resolved CFD–DEM investigation into the onset of suffusion: effect of confining pressure and stress anisotropy. Int. J. Numer. Anal. Methods Geomech. 47 (16), 3018–3043.
Chen, R., Liu, L., Li, Z., Deng, G., Zhang, Y., Zhang, Y., 2021. A novel vertical stress-controlled apparatus for studying suffusion along horizontal seepage through soils. Acta Geotech. 16 (7), 2217–2230.
Chen, R., Luo, Z.-y., Li, A.-g., Wang, H., Liu, L.-l., Zhang, L.-l., 2025. Mesoscopic interpretation of fines clogging-induced permeability changes in completely decomposed granite. Bull. Eng. Geol. Environ. 84 (6), 308.
Chen, J., Zhang, J., 2022. A semi-resolved CFD-DEM coupling model using a two-way domain expansion method. J. Comput. Phys. 469, 111532.
Chen, R., Zhang, L.-L., Deng, G., Chen, Z.-K., Liu, L.-L., Zhou, Z.-L., Luo, Z.-Y., 2024. A large-sized permeameter for studying suffusion characteristics of anisotropic soils. Geotech. Test. J. 47 (3), 631–652.
Coop, M., 1990. The mechanics of uncemented carbonate sands. Géotechnique 40 (4), 607–626.
Cundall, P.A., Strack, O.D.L., 1979. A discrete numerical model for granular assemblies. Géotechnique 30 (3), 331–336.
Ding, H., Wang, X., Wen, D., Huang, P., 2024. Seepage deformation characteristic of gap-graded coral sand in the south China sea. Appl. Ocean Res. 143, 103865.
Ergun, S., Orning, A.A., 1949. Fluid flow through randomly packed columns and fluidized beds. Ind. Eng. Chem. 41 (6), 1179–1184.
Fan, Z., Hu, C., Zhu, Q., Jia, Y., Zuo, D., Duan, Z., 2021. Three-dimensional pore characteristics and permeability properties of calcareous sand with different particle sizes. Bull. Eng. Geol. Environ. 80, 2659–2670.
Fannin, R., Moffat, R., 2006. Observations on internal stability of cohesionless soils. Geotechnique 56 (7), 497–500.
Feng, Y.T., 2021. An energy-conserving contact theory for discrete element modelling of arbitrarily shaped particles: Basic framework and general contact model. Comput. Methods Appl. Mech. Engrg. 373, 113454.
Galindo-Torres, S., Scheuermann, A., Mühlhaus, H., Williams, D., 2015. A micro-mechanical approach for the study of contact erosion. Acta Geotech. 10 (3), 357–368.
Golightly, C., Hyde, A., 2021. Some fundamental properties of carbonate sands. In: Engineering for Calcareous Sediments. Vol. 1, CRC Press, pp. 69–78.

Goniva, C., Kloss, C., Hager, A., Pirker, S., 2010. An open source CFD-DEM perspective. In: Proceedings of OpenFOAM Workshop. GÖteborg, pp. 22–24.
Guo, N., Zhao, J., 2013. The signature of shear-induced anisotropy in granular media. Comput. Geotech. 47, 1–15.
Hager, A., Kloss, C., Pirker, S., Goniva, C., 2014. Parallel resolved open source CFD-DEM: method, validation and application. J. Comput. Multiph. Flows 6 (1), 13–27.
Harmon, J.M., Arthur, D., Andrade, J.E., 2020. Level set splitting in DEM for modeling breakage mechanics. Comput. Methods Appl. Mech. Engrg. 365, 112961.
He, Y., Yan, S., Wang, T., Jiang, B., Huang, Y., 2016. Hydrodynamic characteristics of gas-irregular particle two-phase flow in a bubbling fluidized bed: An experimental and numerical study. Powder Technol. 287, 264–276.
Huang, S., Huang, L., Lai, Z., Zhao, J., 2023. Morphology characterization and discrete element modeling of coral sand with intraparticle voids. Eng. Geol. 315, 107023.
Huang, S., Wang, P., Lai, Z., Yin, Z.-Y., Huang, L., Xu, C., 2024. Machine-learning-enabled discrete element method: The extension to three dimensions and computational issues. Comput. Methods Appl. Mech. Engrg. 432, 117445.
Hwang, S., Pan, J., Fan, L.-S., 2024. Neural-network-based drag force model for polydisperse assemblies of irregular-shaped particles. Powder Technol. 440, 119783.
Ke, L., Takahashi, A., 2014a. Experimental investigations on suffusion characteristics and its mechanical consequences on saturated cohesionless soil. Soils Found. 54 (4), 713–730.
Ke, L., Takahashi, A., 2014b. Triaxial erosion test for evaluation of mechanical consequences of internal erosion. Geotech. Test. J. 37 (2), 347–364.
Kenney, T., Lau, D., 1985. Internal stability of granular filters. Can. Geotech. J. 22 (2), 215–225.
Kézdi, A., 1979. Soil Physics: Selected Topics (Developments in Geotechnical Engineering). Technical Report.
Kodieh, A., Gelet, R., Marot, D., Fino, A., 2021. A study of suffusion kinetics inspired from experimental data: comparison of three different approaches. Acta Geotech. 16, 347–365.
Kong, D., Fonseca, J., 2019. On the kinematics of shelly carbonate sand using X-ray micro tomography. Eng. Geol. 261, 105268.
Lai, Z., Chen, Q., Huang, L., 2020. Fourier series-based discrete element method for computational mechanics of irregular-shaped particles. Comput. Methods Appl. Mech. Engrg. 362, 112873.
Lai, Z., Zhao, S., Zhao, J., Huang, L., 2022. Signed distance field framework for unified DEM modeling of granular media with arbitrary particle shapes. Comput. Mech. 70, 763–783.
Lai, Z., Zhao, J., Zhao, S., Huang, L., 2023. Signed distance field enhanced fully resolved CFD-DEM for simulation of granular flows involving multiphase fluids and irregularly shaped particles. Comput. Methods Appl. Mech. Engrg. 414, 116195.
Li, Z., Zhang, Y., Chen, R., Tai, P., Zhang, Z., 2025. Numerical investigation of morphological effects on crushing characteristics of single calcareous sand particle by finite-discrete element method. Powder Technol. 453, 120592.
Li, Z., Zhang, Z., Tai, P., Shen, P., Li, J., 2024. Investigation of morphological effects on crushing characteristics of calcareous sand particle by 3D image analysis with spherical harmonics. Powder Technol. 433, 119204.
Liu, W., Wan, S., Luo, X., Fu, M., 2020. Experimental study of suffusion characteristics within granite residual soil controlling inflow velocity. Arab. J. Geosci. 13, 1–8.
Liu, Y., Yin, Z.-Y., 2024. Suffusion of irregular concave gap-graded sand with resolved CFD-DEM. Can. Geotech. J..
Liu, Y.-J., Yin, Z.-Y., Huang, S., Lai, Z., Zhou, C., 2024. Resolved CFD-DEM modeling of suffusion in gap-graded shaped granular soils. J. Geotech. Geoenvironmental Eng. 150 (4), 04024008.
Lv, Y., Li, X., Fan, C., Su, Y., 2021. Effects of internal pores on the mechanical properties of marine calcareous sand particles. Acta Geotech. 16 (10), 3209–3228.
Mao, C.-X., 2005. Study on piping and filters : part I of piging. Rock Soil Mech. 26 (2), 209–215, (in Chinese).
Maroof, M.A., Mahboubi, A., Noorzad, A., 2021. Effects of grain morphology on suffusion susceptibility of cohesionless soils. Granul. Matter 23 (1), 8.
Mehdizadeh, A., Disfani, M.M., Evans, R., Arulrajah, A., Ong, D., 2017. Mechanical consequences of suffusion on undrained behaviour of a gap-graded cohesionless soil-an experimental approach. Geotech. Test. J. 40 (6), 1026–1042.
Mehdizadeh, A., Disfani, M.M., Shire, T., 2021. Post-erosion mechanical response of internally unstable soil of varying size and flow regime. Can. Geotech. J. 58 (4), 531–539.
Nan, X., Hou, J., Shen, Z., Tong, Y., Li, G., Wang, X., Kang, Y., 2022. CFD-DEM coupling with multi-sphere particles and application in predicting dynamic behaviors of drifting boats. Ocean Eng. 247, 110368.
Nguyen, C.D., Benahmed, N., Andò, E., Sibille, L., Philippe, P., 2019. Experimental investigation of microstructural changes in soils eroded by suffusion using X-ray tomography. Acta Geotech. 14, 749–765.
Nguyen, V., Nguyen, Q., Zhang, Y., Lim, C., Khoo, B., 2016. Effect of particle size on erosion characteristics. Wear 348, 126–137.
Peng, Y., Yin, Z.-Y., Ding, X., 2022. Analysis of particle corner-breakage effect on pile penetration in coral sand: model tests and DEM simulations. Can. Geotech. J. 60 (5), 749–765.
Richards, K., Reddy, K.R., 2012. Experimental investigation of initiation of backward erosion piping in soils. Géotechnique 62 (10), 933–942.
Shahnazari, H., Rezvani, R., 2013. Effective parameters for the particle breakage of calcareous sands: An experimental study. Eng. Geol. 159, 98–105.
Sibille, L., Lominé, F., Poullain, P., Sail, Y., Marot, D., 2015. Internal erosion in granular media: direct numerical simulations and energy interpretation. Hydrol. Process. 29 (9), 2149–2163.
Skempton, A., Brogan, J., 1994. Experiments on piping in sandy gravels. Géotechnique 44 (3), 449–460.
Slangen, P., Fannin, R., 2017. The role of particle type on suffusion and suffosion. Géotech. Lett. 7 (1), 6–10.
Sobieski, W., 2009. Switch function and sphericity coefficient in the Gidaspow drag model for modeling solid-fluid systems. Dry. Technol. 27 (2), 267–280.
Song, S., Wang, P., Yin, Z., Cheng, Y.P., 2024. Micromechanical modeling of hollow cylinder torsional shear test on sand using discrete element method. J. Rock Mech. Geotech. Eng. 16 (12), 5193–5208.
Wang, T., Cui, Y., Liu, Z., Bao, X., 2025a. Experimental study on particle breakage in calcareous sand during large-displacement shear at soil-structure interfaces. Eng. Geol. 108358.
Wang, C., Ding, X., Yin, Z.-Y., Peng, Y., Chen, Z., 2021. Mechanical characteristics and particle breakage of coral sand under one-dimensional repeated loading. Acta Geotech. 1–14.
Wang, X., Jiao, Y., Wang, R., Hu, M., Meng, Q., Tan, F., 2011. Engineering characteristics of the calcareous sand in Nansha Islands, South China Sea. Eng. Geol. 120 (1–4), 40–47.
Wang, Z., Liu, M., 2021. On the determination of grid size/smoothing distance in un-/semi-resolved CFD-DEM simulation of particulate flows. Powder Technol. 394, 73–82.
Wang, T., Ma, L., Wang, M., Li, Z., Zhang, X., Geng, H., 2022a. Effects of particle shape on dynamic mechanical behaviours of coral sand under one-dimensional compression. Eng. Geol. 304, 106624.
Wang, X., Wang, X., Jin, Z., Zhu, C., Wang, R., Meng, Q., 2017. Investigation of engineering characteristics of calcareous soils from fringing reef. Ocean Eng. 134, 77–86.
Wang, T., Wang, P., Yin, Z.-Y., Laouafa, F., Hicher, P.-Y., 2024. Hydro-mechanical analysis of particle migration in fractures with CFD-DEM. Eng. Geol. 335, 107557.
Wang, T., Wang, P., Yin, Z.-Y., Zhang, F., 2022b. DEM-DFM modeling of suffusion in calcareous sands considering the effect of double-porosity. Comput. Geotech. 151, 104965.
Wang, T., Wang, Z.-Y., Zhang, F., Xu, C., 2025b. DEM-DFM Modeling Suffusion of Granular Soils under Triaxial Compression. Int. J. Geomech. 25 (2), 04024352.
Wang, X., Weng, Y., Wei, H., Meng, Q., Hu, M., 2019. Particle obstruction and crushing of dredged calcareous soil in the Nansha Islands, South China Sea. Eng. Geol. 261, 105274.
Wang, X., Wu, Y., Cui, J., Zhu, C.-Q., Wang, X.-Z., 2020. Shape characteristics of coral sand from the South China Sea. J. Mar. Sci. Eng. 8 (803), 1–24.
Wang, P., Yin, Z.-Y., Hicher, P.-Y., Cui, Y.-J., 2023. Micro-mechanical analysis of one-dimensional compression of clay with DEM. Int. J. Numer. Anal. Methods Geomech. 47 (15), 2706–2724.
Wang, Y., Zhou, L., Wu, Y., Yang, Q., 2018. New simple correlation formula for the drag coefficient of calcareous sand particles of highly irregular shape. Powder Technol. 326, 379–392.
Wen, C.Y., Yu, Y.H., 1966. A generalized method for predicting the minimum fluidization velocity. AIChE J. 12 (3), 610–612.
Xin, L., Zhang, Y., Ma, X., Sun, X., Wei, H., 2024. Particle breakage characteristics of marine coral sand under cyclic shear loading conditions. Int. J. Geomech. 24 (12), 04024283.
Xiong, H., Qiu, Y., Liu, J., Yin, Z.-Y., Chen, X., 2023a. Macro–microscopic mechanism of suffusion in calcareous sand under tidal fluctuations by coupled CFD-DEM. Comput. Geotech. 162, 105676.
Xiong, H., Sun, J., Chen, F., Yin, Z.-Y., Chen, X., 2023b. Suffusion behavior of crushed calcareous sand under reversed cyclic hydraulic conditions. Constr. Build. Mater. 408, 133817.
Xiong, H., Wu, H., Bao, X., Fei, J., 2021a. Investigating effect of particle shape on suffusion by CFD-DEM modeling. Constr. Build. Mater. 289, 123043.
Xiong, H., Yin, Z.-Y., Zhao, J., Yang, Y., 2021b. Investigating the effect of flow direction on suffusion and its impacts on gap-graded granular soils. Acta Geotech. 16, 399–419.
Yan, L., Zhang, X., Liu, X., Gao, H., Zhou, Z., Wang, G., 2025. Multi-scale analysis of pore structure and permeability simulation of coral gravel under particle breakage using X-ray computerized tomography. Granul. Matter 27 (3), 1–19.
Yang, J., Balaras, E., 2006. An embedded-boundary formulation for large-eddy simulation of turbulent flows interacting with moving boundaries. J. Comput. Phys. 215 (1), 12–40.